DOE/BC/14895-13 (Vol III)
(DE96001282)

GEOSCIENCE/ENGINEERING CHARACTERIZATION OF THE INTERWELL ENVIRONMENT IN CARBONATE RESERVOIRS BASED ON OUTCROP ANALOGS, PERMIAN BASIN, WEST TEXAS AND NEW MEXICO-STRATIGRAPHIC HIERARCHY AND CYCLE STACKING FACIES DISTRIBUTION, AND INTERWELL-SCALE HETEROGENEITY: GRAYBURG FORMATION, NEW MEXICO

Final Report

By
Roger J. Barnaby
W. Bruce Ward
James W. Jennings, Jr.

June 1997

Performed Under Contract No. DE-AC22-93BC14895

The University of Texas at Austin
Bureau of Economic Geology
Austin, Texas

National Petroleum Technology Office
U. S. DEPARTMENT OF ENERGY
Tulsa, Oklahoma

DOE/BC/14895-13 (Vol III)
Distribution Category UC-122

Geoscience/Engineering Characterization Of The Interwell Environment In Carbonate Reservoirs Based On Outcrop Analogs, Permian Basin, West Texas And New Mexico- Stratigraphic Hierarchy And Cycle Stacking Facies Distribution, And Interwell-Scale Heterogeneity: Grayburg Formation, New Mexico

Final Report

By
Roger J. Barnaby
W. Bruce Ward
James W. Jennings, Jr.

June 1997

Work Performed Under Contract No. DE-AC22-93BC14895

Prepared for
U.S. Department of Energy
Assistant Secretary for Fossil Energy

Robert E. Lemmon, Project Manager
National Petroleum Technology Office
P.O. Box 3628
Tulsa, OK 74101

Prepared by:
The University of Texas at Austin
Bureau of Economic Geology
Austin, Texas

TABLE OF CONTENTS

Figures

ABSTRACT

The Grayburg Formation (middle Guadalupian) is a major producing interval in the Permian Basin and has yielded more than 2.5 billion barrels of oil in West Texas. Grayburg reservoirs have produced, on average, less than 30 percent of their original oil in place and are undergoing secondary and tertiary recovery. Efficient design of such enhanced recovery programs dictates improved geological models to better understand and predict reservoir heterogeneity imposed by depositional and diagenetic controls.

The Grayburg records mixed carbonate-siliciclastic sedimentation on shallow-water platforms that rimmed the Delaware and Midland Basins. Grayburg outcrops in the Guadalupe and Brokeoff Mountains region on the northwest margin of the Delaware Basin present an opportunity to construct a detailed, three-dimensional image of the stratigraphic and facies architecture. This model can be applied towards improved description and characterization of heterogeneity in analogous Grayburg reservoirs.

Four orders of stratigraphic hierarchy are recognized in the Grayburg Formation. The Grayburg represents a long-term composite sequence composed of four high-frequency sequences (HFS 1–4). Each HFS contains several composite cycles comprising two or more cycles that define intermediate-scale transgressive-regressive successions. Cycles are the smallest scale upward-shoaling vertical facies successions that can be recognized and correlated across various facies tracts. Cycles thus form the basis for establishing the detailed chronostratigraphic correlations needed to delineate facies heterogeneity.

Grayburg HFS 1 unconformably overlies the top of the San Andres Formation, a major regional sequence boundary. Grayburg HFS 1 and 2 record increased accommodation during long-term transgression. A widespread fusulinid-rich unit at the base of HFS 3 records regional maximum flooding in the Grayburg composite sequence. This flooding event is recognized throughout the Permian Basin in outcrop and subsurface. The remaining portion of HFS 3 and all of HFS 4 reflect decreased accommodation during late highstand. A similar stratigraphic

organization is recognized in equivalent Grayburg strata in the subsurface of the Central Basin Platform. The top of the Grayburg is a regional sequence boundary that records a fall in relative sea level prior to Queen deposition.

The stratigraphic setting strongly influenced the distribution and heterogeneity of permeable reservoir facies. For example, TST grainstone facies are highly heterogeneous and formed dip-elongate channels and bars, reflecting a tidal-dominated setting during transgression, accompanied by a rapid increase in accommodation that resulted in high preservation potential of individual facies bodies. Conversely, HST ooid grainstones formed strike-elongate shoals that are laterally continuous along dip and across strike and record reworking and amalgamation of grainstone bodies in an accommodation-limited HST setting. This relationship between stratigraphic position and facies heterogeneity can be utilized to improve subsurface correlations and to better predict facies distribution and lateral dimensions.

Lateral porosity and permeability heterogeneity within potential reservoir flow units was evaluated by core plug sampling along dip-oriented traverses. Semivariograms for these data display a large component of short-range (less than 150 ft) variance with a significant correlation structure at a range between one inch and 5 feet. The variograms display a smaller component of variability with possible long-range correlation structures at separation distances approaching the 500- to 600-ft-long sample traverses.

INTRODUCTION

Carbonate and siliciclastic rocks of the Late Permian Grayburg Formation (Fig. 1) accumulated on shallow-water platforms that flanked the Delaware and Midland Basins (Fig. 2). The Grayburg is a major hydrocarbon producer in the Permian Basin (Fig. 1) and has yielded more than 2.5 billion barrels of oil in West Texas. Because recovery efficiencies average less than 30 percent, it is estimated that more than 3.0 billion barrels of mobile oil remain in these reservoirs

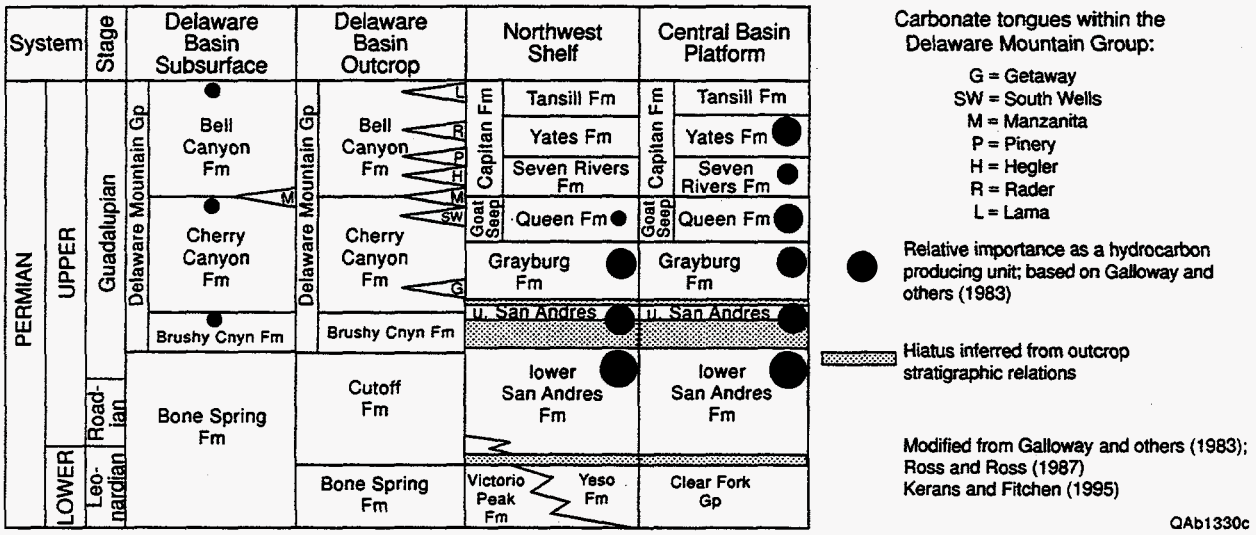

Figure 1. Stratigraphy of uppermost Leonardian through Guadalupian strata of the Permian Basin showing relative importance as a hydrocarbon producing unit (from Kerans and Fitchen, 1995). The Grayburg is an important producer and has yielded 2.5 billion barrels of oil from reservoirs in West Texas.

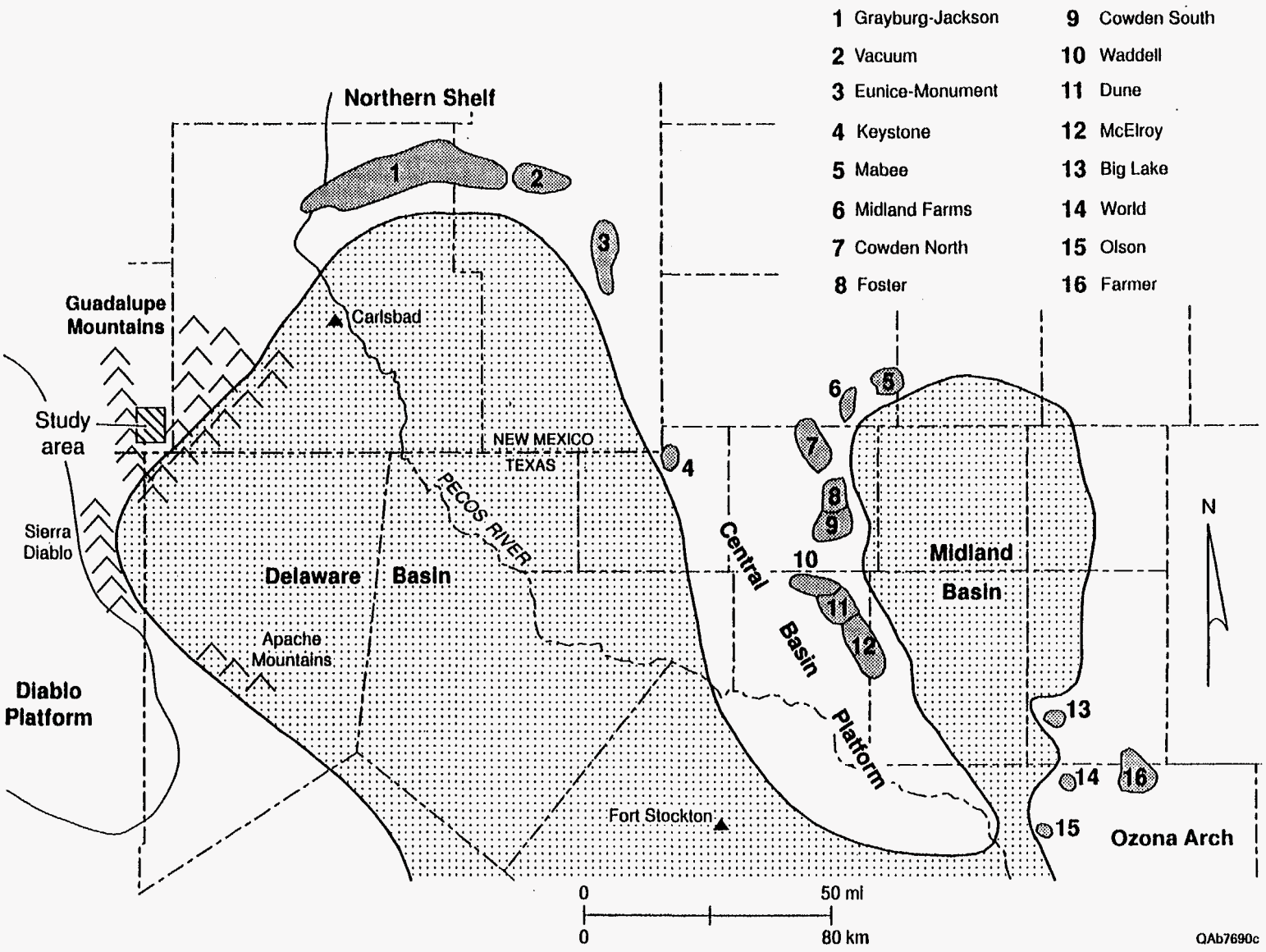

Figure 2. Regional setting during Grayburg deposition (modified from Kerans and Nance, 1991; Ward and others, 1986). Major producing reservoirs (more than 10 million barrels cumulative production) occur along the eastern margin of the Midland Basin, the northern shelf of the Delaware Basin, and on the Ozona Arch. The outcrop analog study is on the northwestern shelf of the Delaware Basin.

(Holtz, pers. comm., 1996). Efficient recovery of this remaining resource dictates a thorough understanding of geological heterogeneity imposed by depositional and diagenetic controls.

The need to describe and characterize reservoir heterogeneity at all scales has been the impetus for detailed outcrop studies of Permian strata in the Guadalupe and Brokeoff Mountains region (Figs. 2 and 3) by the Reservoir Characterization Research Laboratory (RCRL) at the Bureau of Economic Geology. Through synthesis of previous research as well as RCRL stratigraphic studies, Kerans and others (1992a; 1993) constructed a high-frequency sequence stratigraphic framework of the Leonardian through Guadalupian carbonate platform succession in this region (Fig. 4). Detailed investigations of San Andres Formation outcrops document the applicability of sequence stratigraphic concepts to reservoir-scale outcrop studies (Kerans and others, 1994).

The high-resolution chronostratigraphic correlations obtainable from outcrop can be used to build detailed models of geological heterogeneity that are applicable to equivalent subsurface reservoirs. Such an integrated outcrop- and subsurface-oriented approach is essential to accurately describe and characterize hydrocarbon reservoirs. Major issues include: (1) establishing a chronostratigraphic framework for reservoir correlation, (2) delineating facies geometries and dimensions, and (3) modeling reservoir heterogeneity (Kerans and others, 1994).

Previous RCRL investigations of Grayburg Formation outcrops include a regional sequence stratigraphic study by Kerans and Nance (1991). Detailed outcrop characterization studies of Grayburg strata in Stone Canyon are summarized in Nance (1992). Hovorka and others (1993) describe petrographic and petrophysical investigations of core plugs from Stone Canyon.

Barnaby and Ward (1995) present an interim report of the Grayburg stratigraphy in the Brokeoff Mountains region (Figs. 3–6) based on the first year of field work; this report summarizes all of the work completed on this project to date. From outcrop, four high-frequency sequences (Grayburg HFS 1 to 4) are recognized; these are correlative to the four high-frequency sequences recognized in the subsurface. A representative high-frequency sequence, Grayburg HFS 2 (Fig. 7), was selected for detailed outcrop stratigraphic analysis to document interwell-scale (less than hundred to thousands of feet) depositional heterogeneity. Because stratigraphic units and

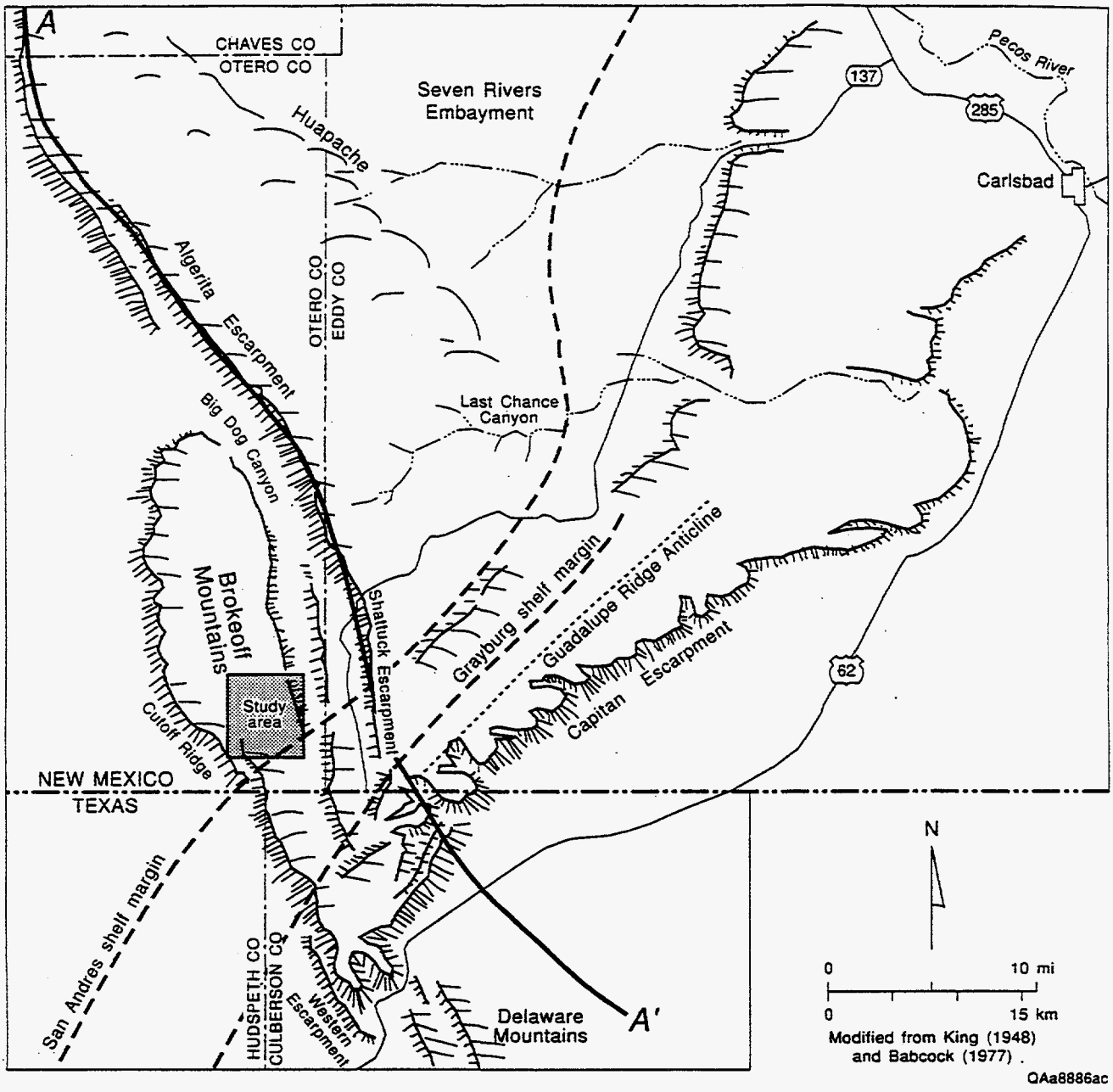

Figure 3. Physiographic map of the Guadalupe and Brokeoff Mountains region, modified from Fitchen (1992). The outcrop study area (rectangle) is bankward of the underlying San Andres margin and is several miles landward of the inferred location of the Grayburg margin. Line A-A′ delineates the general location of the cross section of Kerans and others (1993) shown in Figure 4.

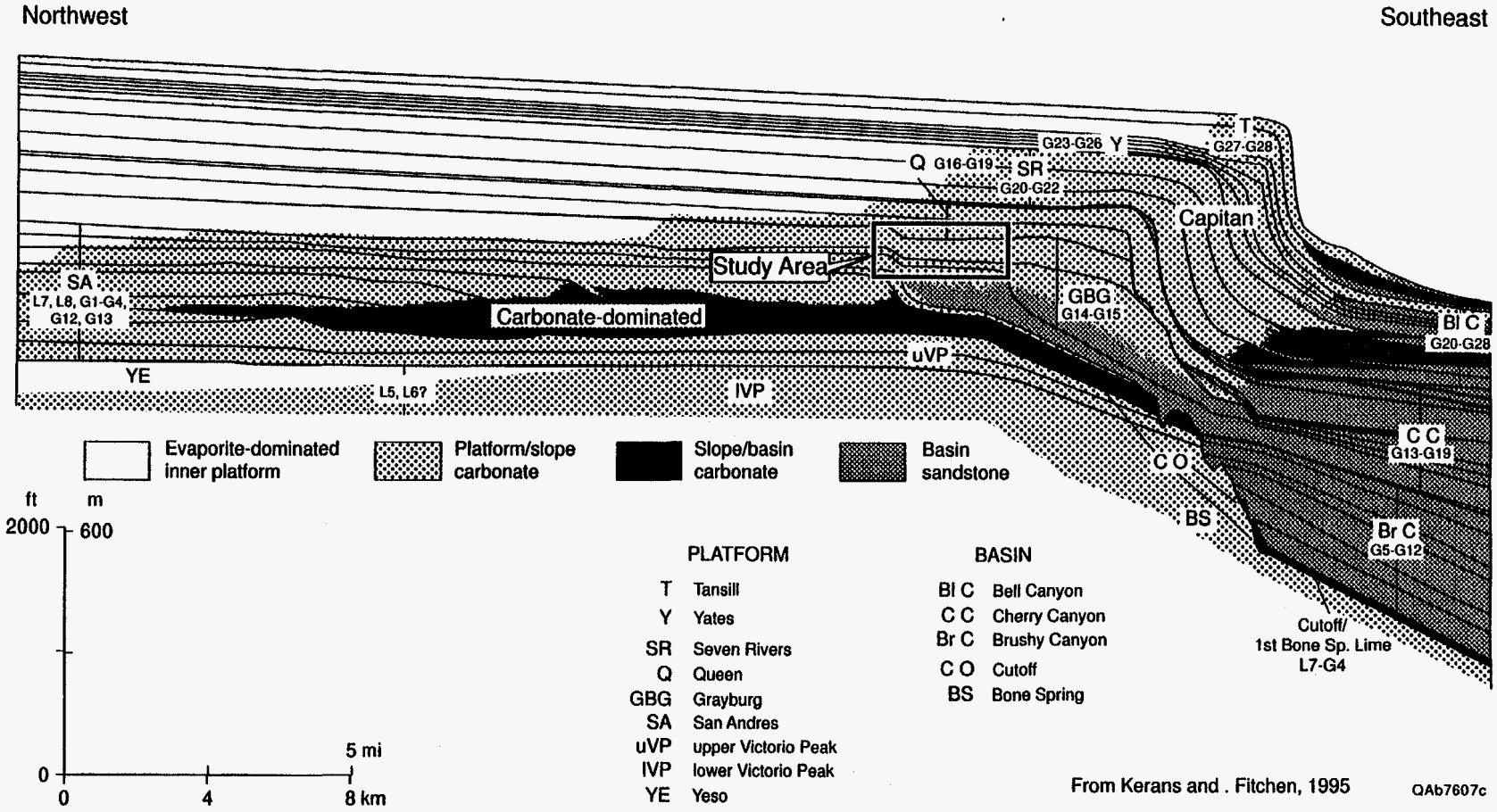

Figure 4. Stratigraphic framework of the Leonardian through Guadalupian carbonate platform succession in the Guadalupe and Brokeoff Mountains region, compiled by Kerans and others (1992a; 1993) and updated by more recent studies. The Grayburg study area is landward of the San Andres and Grayburg platform margins.

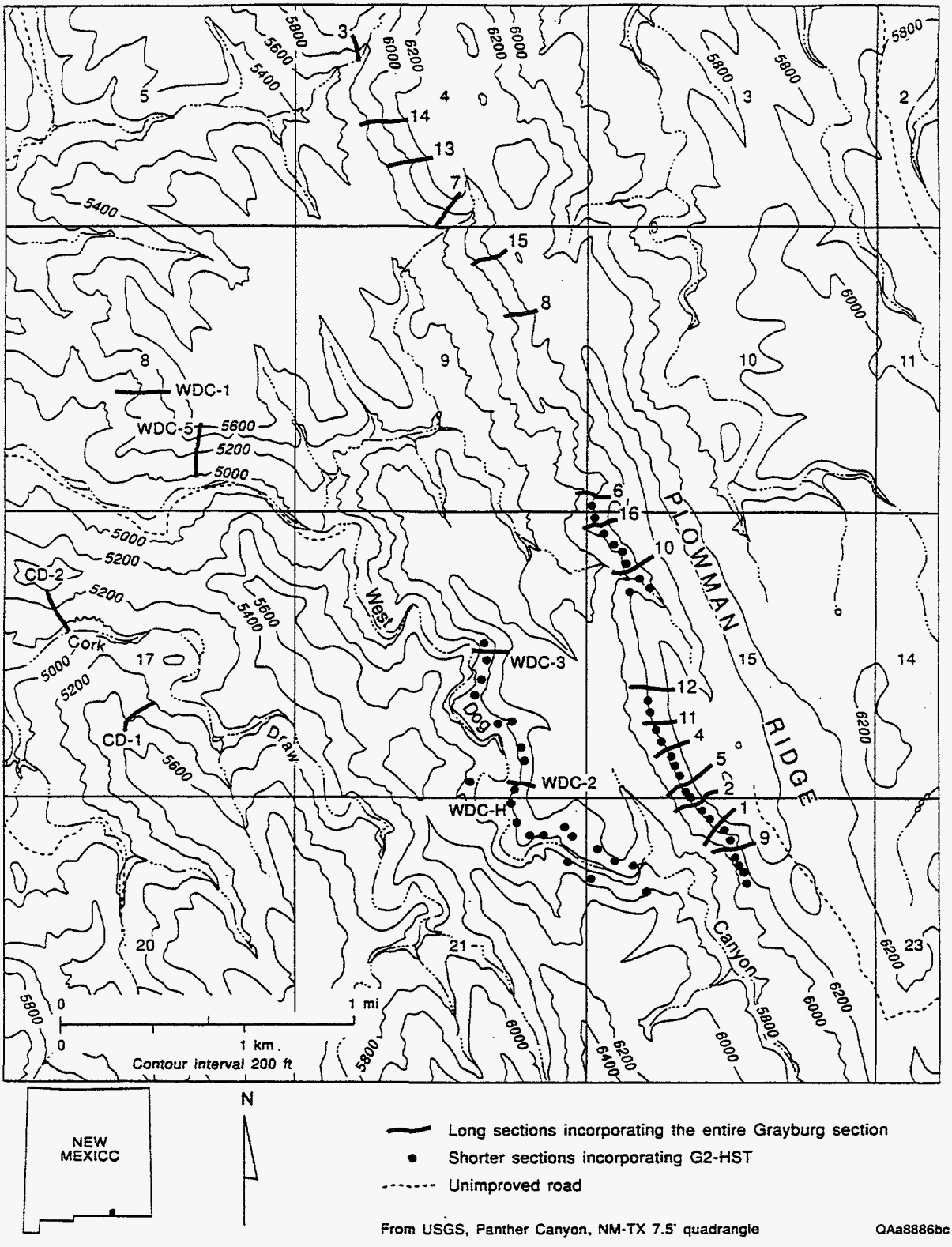

Figure 5. Topographic map of study area showing locations of 22 sections (indicated as lines) of the entire Grayburg interval that were measured at Plowman Ridge, West Dog Canyon (WDC), and Cork Draw (CD). Forty-eight shorter sections (indicated as dots) were measured at Plowman Ridge and West Dog canyon of HFS 2.

Figure 6. Aerial photograph of study area in the Brokeoff Mountains shows the location of depositional dip-oriented Grayburg exposures on Plowman Ridge and West Dog Canyon.

component facies bodies are three-dimensional features, both strike and dip data are needed to define their true extent. Grayburg exposures along the ridges and canyons in the Brokeoff Mountains (Figs. 5 and 6) represent one of a few areas where such a three-dimensional stratigraphic study is possible.

A companion study of the Grayburg Formation in South Cowden field delineates a similar sequence architecture (Ruppel and Bebout, 1995). However, conventional subsurface wireline log, core, seismic, and engineering data do not permit the detailed characterization of facies heterogeneity afforded by the outcrops. This procedure of using outcrops to understand and constrain geologic heterogeneity in subsurface reservoirs forms a foundation for future reservoir characterization studies in the Grayburg.

Petrophysical heterogeneity within potential reservoir flow units was addressed by collecting core plug samples along dip-oriented traverses. Such data is needed to define geostatistical relationships that can be utilized to establish and evaluate models for porosity and permeability distribution used in subsurface reservoirs.

METHODS AND DATA

The Grayburg Formation data and interpretations presented in this paper are based on more than 13,500 ft of section measured at Plowman Ridge, West Dog Canyon, and Cork Draw in the Brokeoff Mountains in southeastern Otero County, New Mexico (Figs. 3–6). Although all precursor limestones were replaced by dolomite, original rock fabrics typically are well-preserved and major facies can be readily identified in the field. Facies were described from outcrop in conjunction with standard petrographic thin sections.

Carbonate rocks were described using Dunham's (1962) classification system with Lucia's (1995) modification that subdivides packstones into mud-dominated and grain-dominated fabrics. Distinguishing between mud-dominated and grain-dominated packstones, however, can be difficult in the field. To discriminate between these packstone fabrics, sedimentary structures were utilized

in conjunction with hand-lens examination of freshly broken rock surfaces. In general, mud-dominated packstones are burrowed to massive units that display smooth concoidal fractures with no visible interparticle pores or cement on freshly broken rock surfaces. Grain-dominated packstones are less bioturbated units with relict cross-lamination that exhibit preserved interparticle pores or cement and/or sucrosic textures on freshly broken rock surfaces. These two packstone fabrics are transitional in nature and commonly exhibit complex interfingering relationships. The two fabrics were lumped together for larger-scale stratigraphic mapping with the exception of the window of detailed mapping for HFS 2 on Plowman Ridge.

Initial stratigraphic analysis of the entire Grayburg Formation was based on exposures from Plowman Ridge, a 4-mi-long, north-trending ridge that parallels depositional dip (Figs. 5 and 6). Kerans and Fitchen (unpublished data, 1993) originally measured and described a vertical section on the southern end of Plowman Ridge. We measured additional sections of the entire Grayburg interval from Plowman Ridge, West Dog Canyon, and Cork Draw.

Detailed stratigraphic analysis and mapping of facies complexity within the cycle-scale chronostratigraphic framework focused on Grayburg HFS 2 (100-120 ft thick) on Plowman Ridge and West Dog Canyon (Figs. 5 and 6), 0.5 mi. west of Plowman Ridge, across depositional strike. Within each window, correlations are based on closely spaced (100 to 400 ft) measured sections required for high-resolution correlation and to delineate interwell-scale facies heterogeneity. Cycle tops and major lithofacies were physically correlated between sections by walking out cycle tops, bedding surfaces and facies contacts, and by tracing the stratal relationships on large scale (1:100 to 1:200) oblique photographs. The high-resolution stratigraphic framework allowed confident correlation of each cycle between the two dip-oriented sections.

Petrophysical and petrographic analysis is based on nearly 700 1-inch-diameter core plugs. Two vertical plug traverses were collected, one from the entire Grayburg interval on Plowman Ridge and another from HFS 2 in West Dog Canyon. Four horizontal core plug traverses from Grayburg HFS 2 were collected from two potential reservoir flow units in Grayburg HFS 2 from Plowman Ridge and West Dog Canyon. These core plug samples were collected at 5 ft intervals

along 500 to 600 ft horizontal transects of: (1) an ooid grain-dominated dolopackstone unit in cycle 10; and (2) an ooid dolograinstone unit capping cycle 12. From each plug, helium porosity and air permeability were determined and thin sections were subjected to standard petrographic analysis.

REGIONAL GEOLOGICAL SETTING AND SEQUENCE STRATIGRAPHY

Geological Setting

The Grayburg Formation (middle Guadalupian) records mixed carbonate-siliciclastic sedimentation on shallow-water platforms that rimmed the Delaware and Midland Basins. Major Grayburg reservoirs flank the margins of the eastern Central Basin Platform, the Ozona Arch, and the Northern Shelf of the Delaware Basin (Fig. 2). Equivalent Grayburg strata exposed in the Guadalupe and Brokeoff Mountains region on the Northwestern Shelf of the Delaware Basin (Figs. 2 and 3) present an opportunity to conduct detailed stratigraphic analysis of analogous outcrops and construct a three-dimensional image of the stratigraphic and facies architecture.

On the northwestern rim of the Delaware Basin, shallow-water Grayburg carbonate and siliciclastic strata grade landward into inner platform evaporite-dominated facies and are flanked basinward by the siliciclastic Cherry Canyon Formation (Fig. 4). The Grayburg ranges in thickness from 260 ft in its most landward exposure and thickens towards the platform margin to more than 1,200 ft (Fekete and others, 1986; Franseen and others, 1989; Kerans and Nance, 1991; Kerans and others, 1992a; 1993). This study focused on relatively flat-lying Grayburg platform strata that accumulated landward of the platform margins for the underlying uppermost San Andres Formation and the Grayburg Formation (Figs. 3 and 4). In the study area, the Grayburg ranges from 300 ft in thickness in the most landward location and thickens basinward to 600 ft at the southern terminus of Plowman Ridge.

Approximately 10 miles basinward of the study area, the Grayburg attains a maximum thickness of more than 1,200 ft along the Western Escarpment. At this location, the Grayburg

margin is truncated by an erosional surface with an estimated minimum relief of 650 to 1,000 ft (Fekete and others, 1986; Franseen and others, 1989). Erosional removal of the platform margin makes it difficult to determine its precise location or to ascertain whether the margin exhibited a ramp or a rimmed shelf morphology (*sensu* Read, 1985).

Sequence Stratigraphic Framework

Following the original definition of the Grayburg Formation from an oil well in northeast Eddy County, New Mexico (Dickey, 1940), an outcrop type section was proposed for the Grayburg in the Sitting Bull Falls area of the Guadalupe Mountains (Moran, 1954). Boyd (1958) conducted the first comprehensive geological mapping of Permian strata in the Brokeoff Mountains, Algerita Escarpment, and Shattuck Valley areas. The stratigraphic interpretations of Boyd (1958) for the San Andres, Grayburg, and Queen Formations were redefined by Hayes (1959; 1964), who consistently correlated and mapped these formations along Algerita Escarpment and Shattuck Valley and extended the geological mapping by Boyd (1958) to the north and east throughout the central Guadalupes.

A modern sequence stratigraphic framework for the Grayburg Formation in the Guadalupe Mountains region initially was presented by Sarg and Lehmann (1986). The San Andres-Grayburg formational contact was interpreted to represent a regional sequence boundary between the erosional toplap surface above uppermost San Andres progradational clinoforms and onlapping siliciclastic-dominated strata of the lowermost Grayburg. The Grayburg was designated as a 3rd order sequence. The top of the Grayburg was interpreted to be a regional sequence boundary at the base of the Queen Formation (Sarg and Lehmann, 1986).

The regional sequence boundary at the San Andres/Grayburg formational contact (Sarg and Lehmann, 1986) locally displays subaerial exposure features, including erosional truncation, sandstone-filled grikes, paleokarst dissolution dolines and mantling lithoclast breccias (Kerans and Nance, 1991). A major fall in relative sea level (100 to 200 ft or more in magnitude) following San Andres deposition is indicated by stratal and facies relationships (Kerans and Nance, 1991,

Sonnenfeld, 1991; Kerans and Fitchen, 1995; this study) and by paleotopographic relief on the exposure surface indicated by sandstone-filled paleokarst and grikes (Fitchen, 1993).

In the Brokeoff Mountains region examined by this study, the San Andres/Grayburg sequence boundary caps the erosional toplap surface above uppermost San Andres progradational clinoforms (Fitchen, 1993). Above the toplap surface, local paleokarst dissolution dolines and sandstone-filled grikes extend at least 30 ft below the sequence boundary, and the relief on the karsted sloping surface of the San Andres/Grayburg sequence boundary attests to a minimum fall in sea level of 100 ft. Basal onlapping Grayburg strata are composed of dominantly trough-cross-stratified to massive quartz sandstones with abundant breccia fragments of micritic dolomite.

Kerans and Nance (1991) subdivided the 3rd order Grayburg sequence of Sarg and Lehmann (1986) into lowstand/transgressive and highstand systems tracts. They considered the Grayburg to represent a long-term accommodation cycle with transgressive fusulinid-bearing, outer ramp facies at the base recording successive flooding of the platform during sea-level rise and the uppermost strata dominated by tidal flat, grainstone, and grain-dominated packstone facies recording platform aggradation and progradation during the late highstand. Kerans and others (1992a; 1993) reinterpreted the Grayburg to be a composite sequence composed of two high-frequency sequences (Guadalupian HFS 14 and 15), and placed the maximum flooding surface of Kerans and Nance (1991) at the transgressive base of Guadalupian HFS 15. This maximum flooding event is recorded by a widespread fusulinid-bearing packstone/wackestone unit that is recognized throughout the Permian Basin in outcrop and in the subsurface.

We subdivide the Grayburg composite sequence (Figs. 7–11) into four high-frequency sequences (HFS 1–4) that are defined by transgressive-regressive relationships, lateral tracing of unconformable surfaces, facies tract (see Fig. 12) offsets, and vertical facies successions and cycle stacking patterns expressed along a dip cross-section. Grayburg HFS 2 was subjected to detailed stratigraphic analysis (Figs. 13 and 14) discussed below. Correlation of our stratigraphic framework with previous Grayburg studies in this region (Kerans and Nance, 1991; Kerans and others, 1992a; 1993) indicates that our Grayburg HFS 1 and 2 are equivalent with Guadalupian

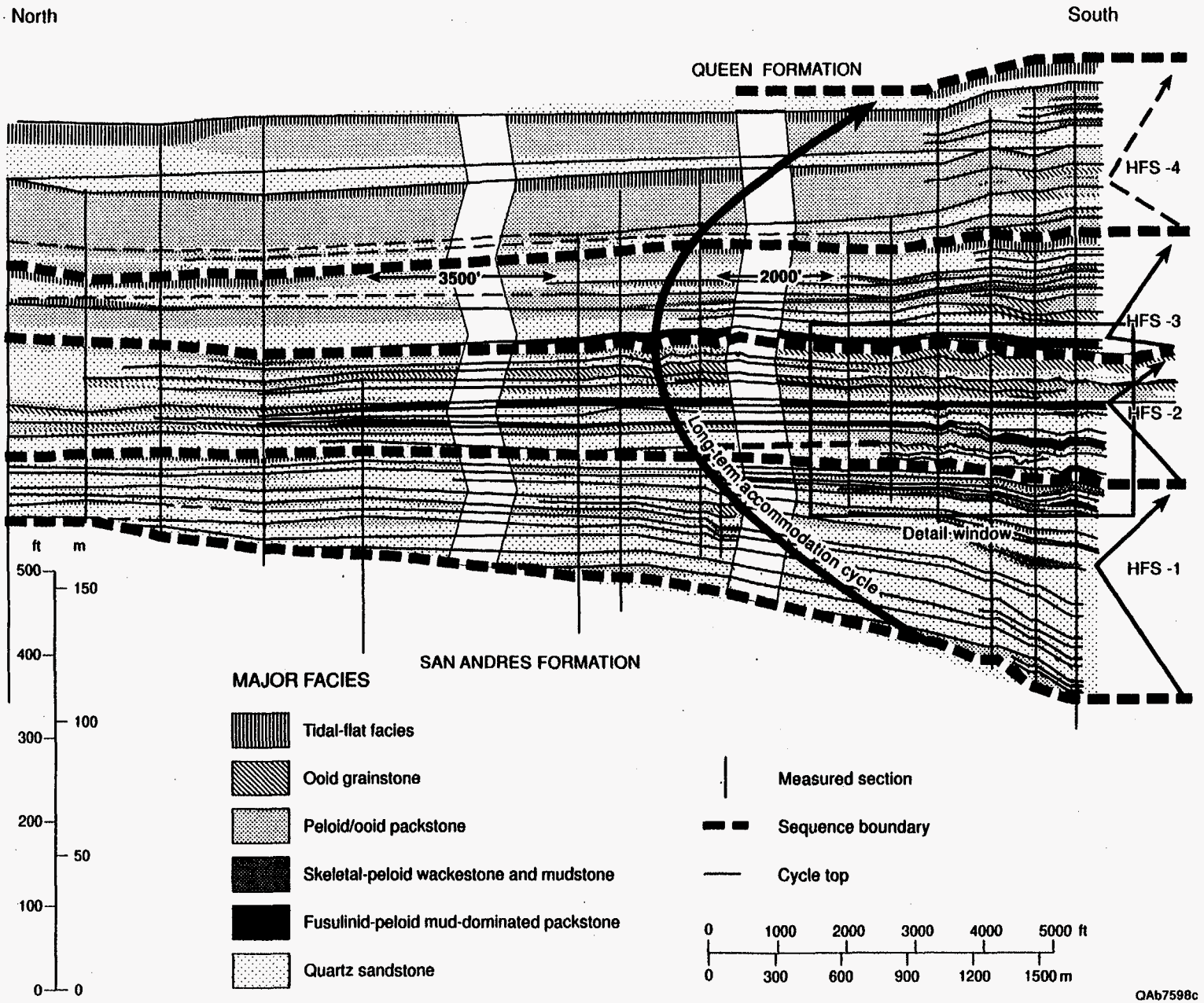

Figure 7. Grayburg stratigraphic framework from dip-parallel exposures on Plowman Ridge. Vertical black lines delineate measured section locations; vertical white bands indicate missing section due to lack of outcrop exposures. Four high-frequency sequences are recognized from the outcrops (HFS 1–4).

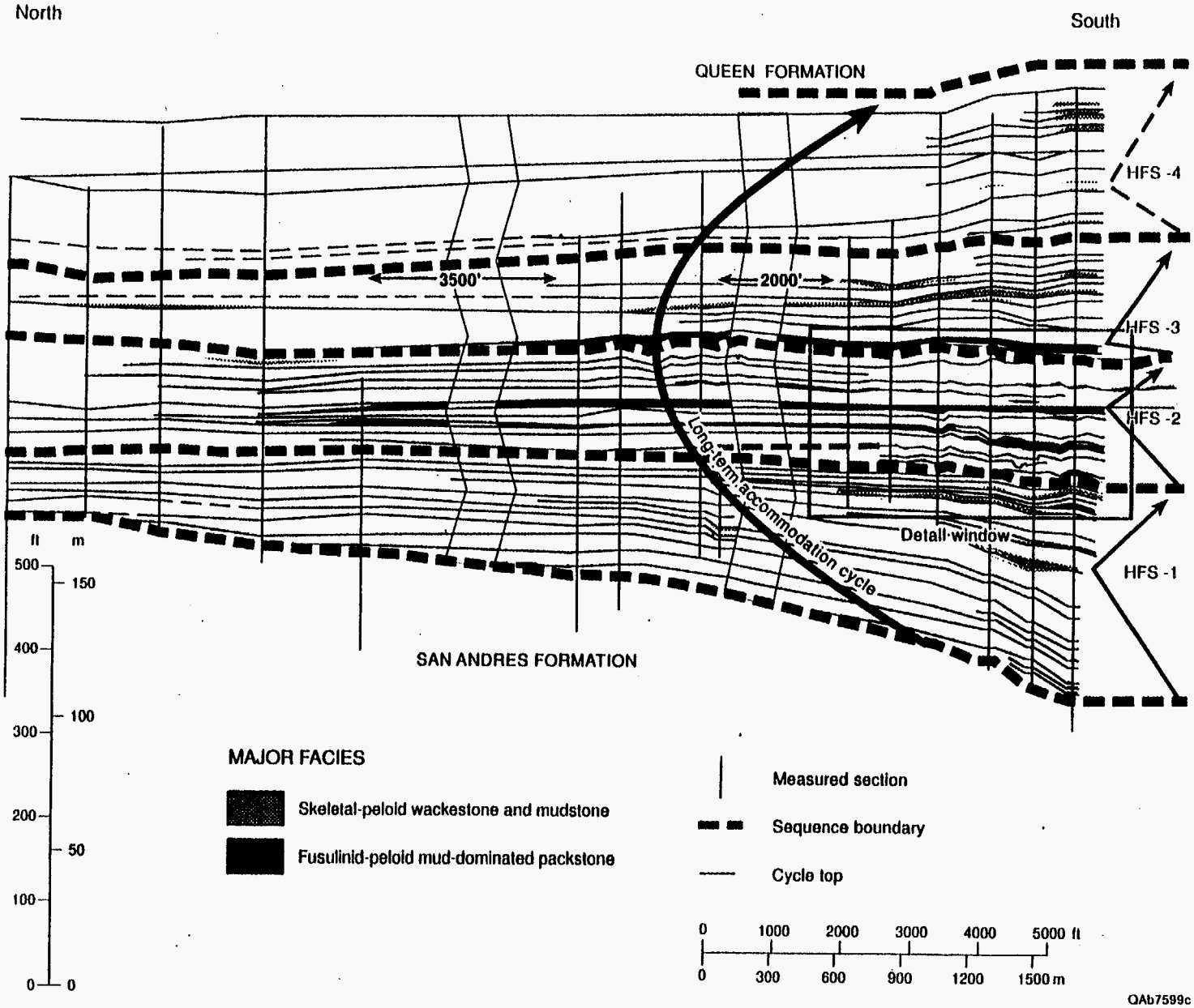

Figure 8. Grayburg stratigraphic framework from outcrop (see Fig. 7). The distribution of outer ramp fusulinid-peloid mud-dominated packstone and skeletal-peloid wackestone and mudstone facies is shown to emphasize the major transgressive events. These transgressions were crucial for defining accommodation trends and the high-frequency sequence stratigraphic framework.

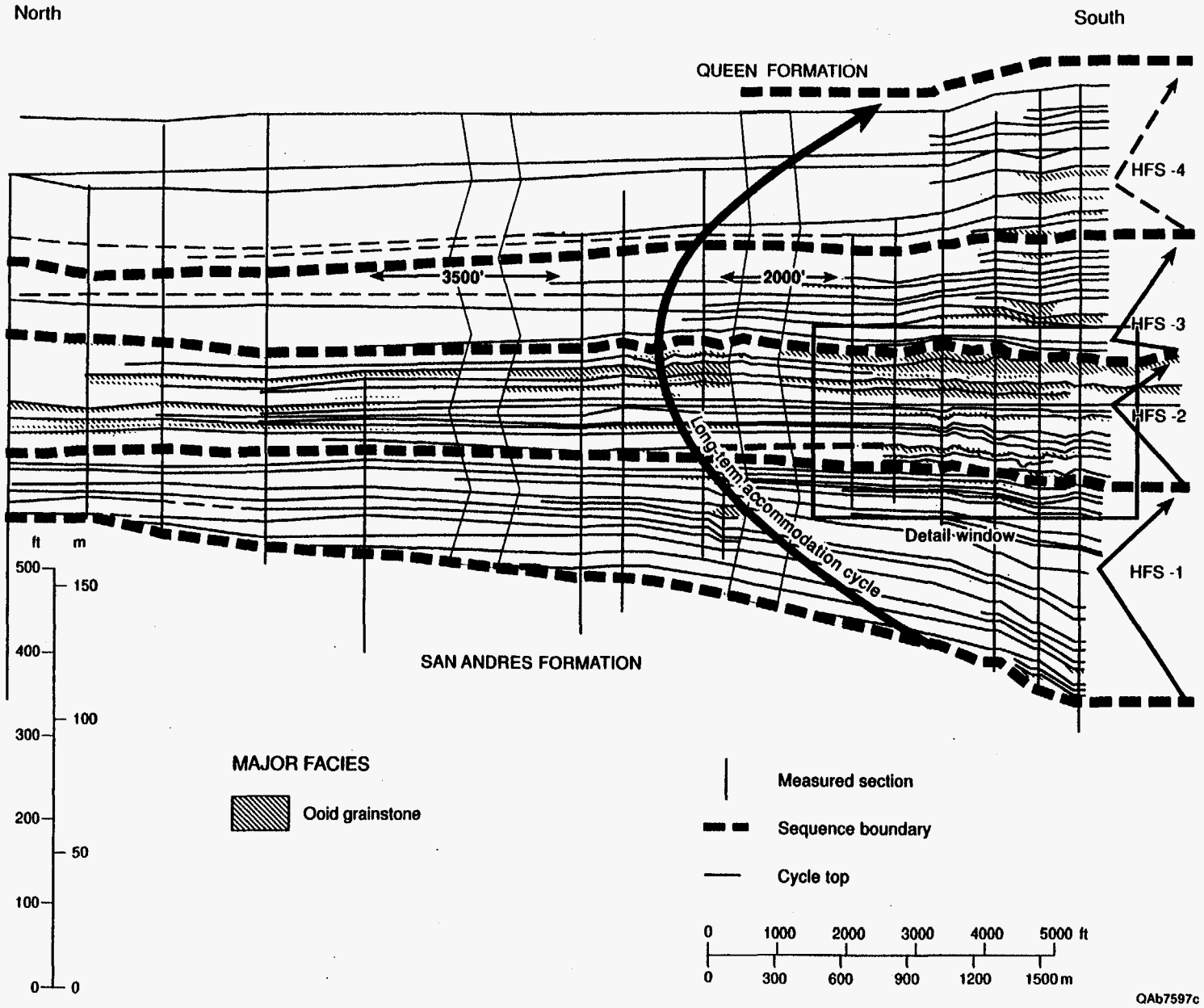

Figure 9. Grayburg stratigraphic framework from outcrop (see Fig. 7). The distribution of ramp crest ooid grainstones is shown to emphasize their preferential development in HFS 2 as well as the lateral facies offsets (landward-stepping vs. seaward-stepping) that reflect intermediate-term cyclicity recorded by the high-frequency sequences.

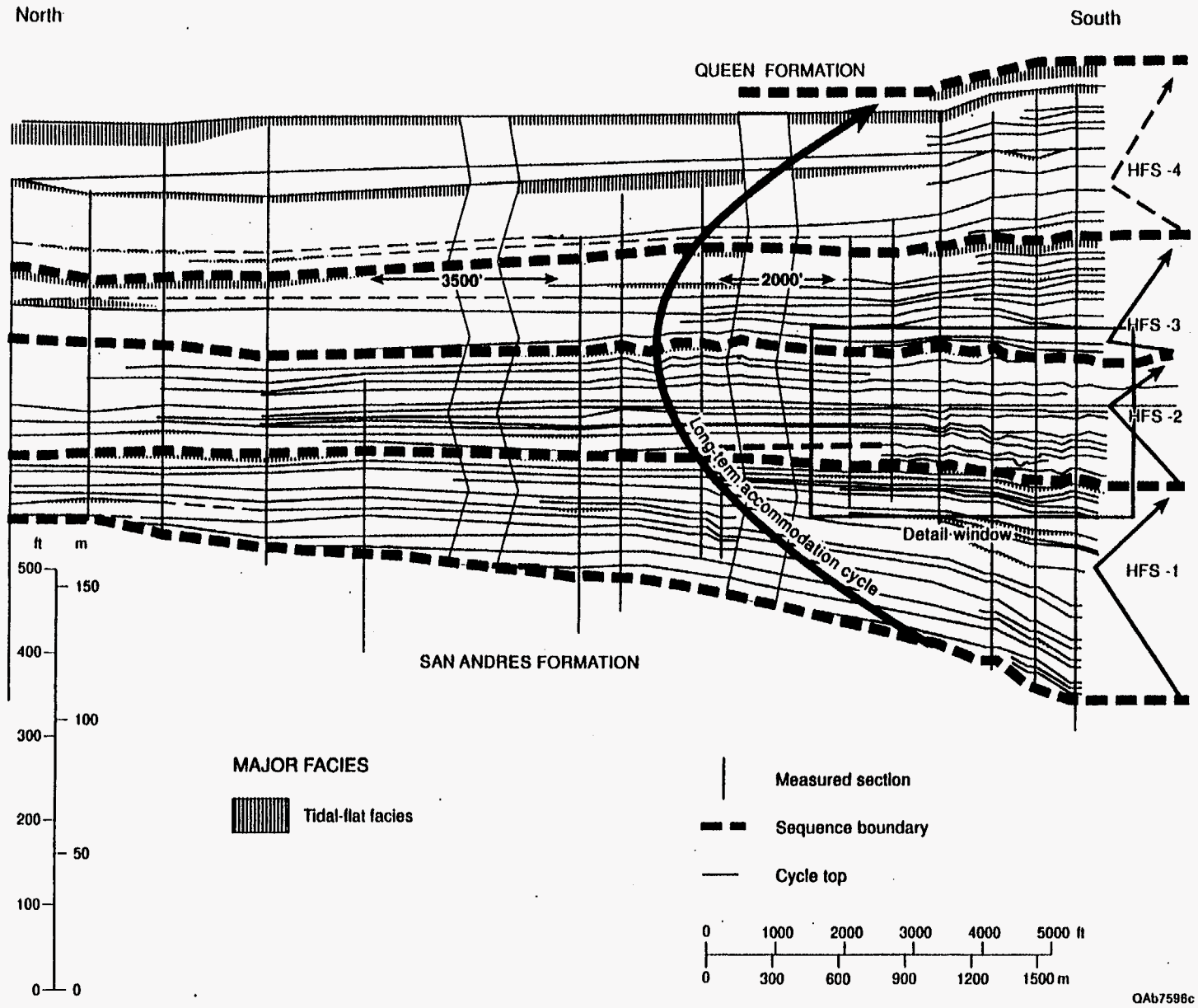

Figure 10. Grayburg stratigraphic framework from outcrop (see Fig. 7). The distribution of tidal flat facies is shown to emphasize episodes of platform aggradation to sea level and complete filling of accommodation.

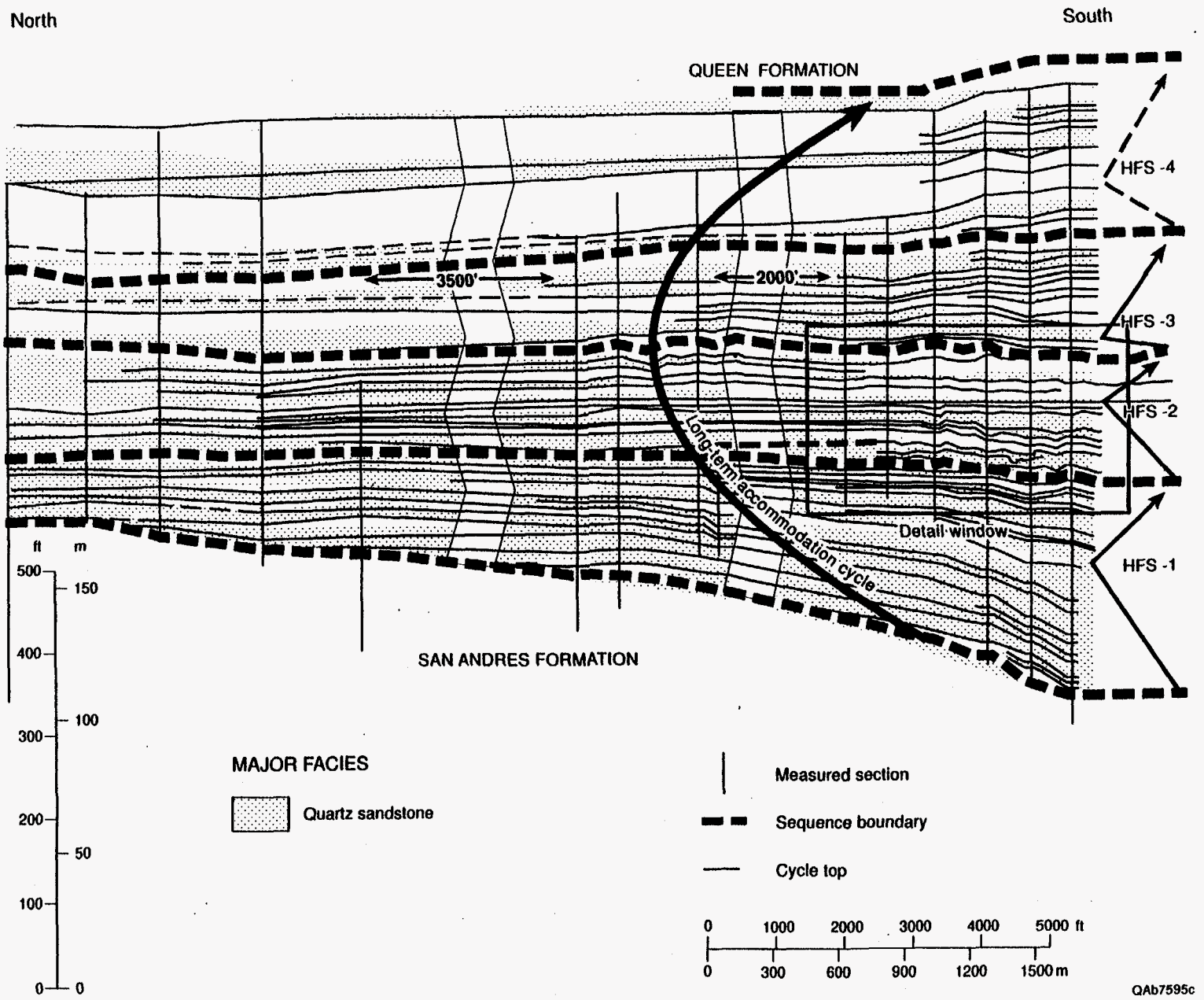

Figure 11. Grayburg stratigraphic framework from outcrop (see Fig. 7). The distribution of quartz sandstones is shown to emphasize periods of prolonged emergence, which facilitated eolian transport of quartz sand to the outer platform.

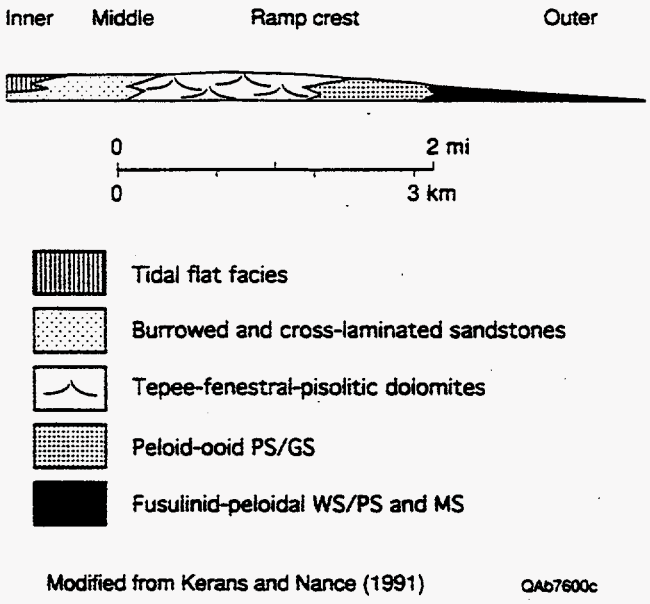

Figure 12. Generalized Grayburg ramp profile and facies tracts of the study area (from Kerans and Nance, 1991).

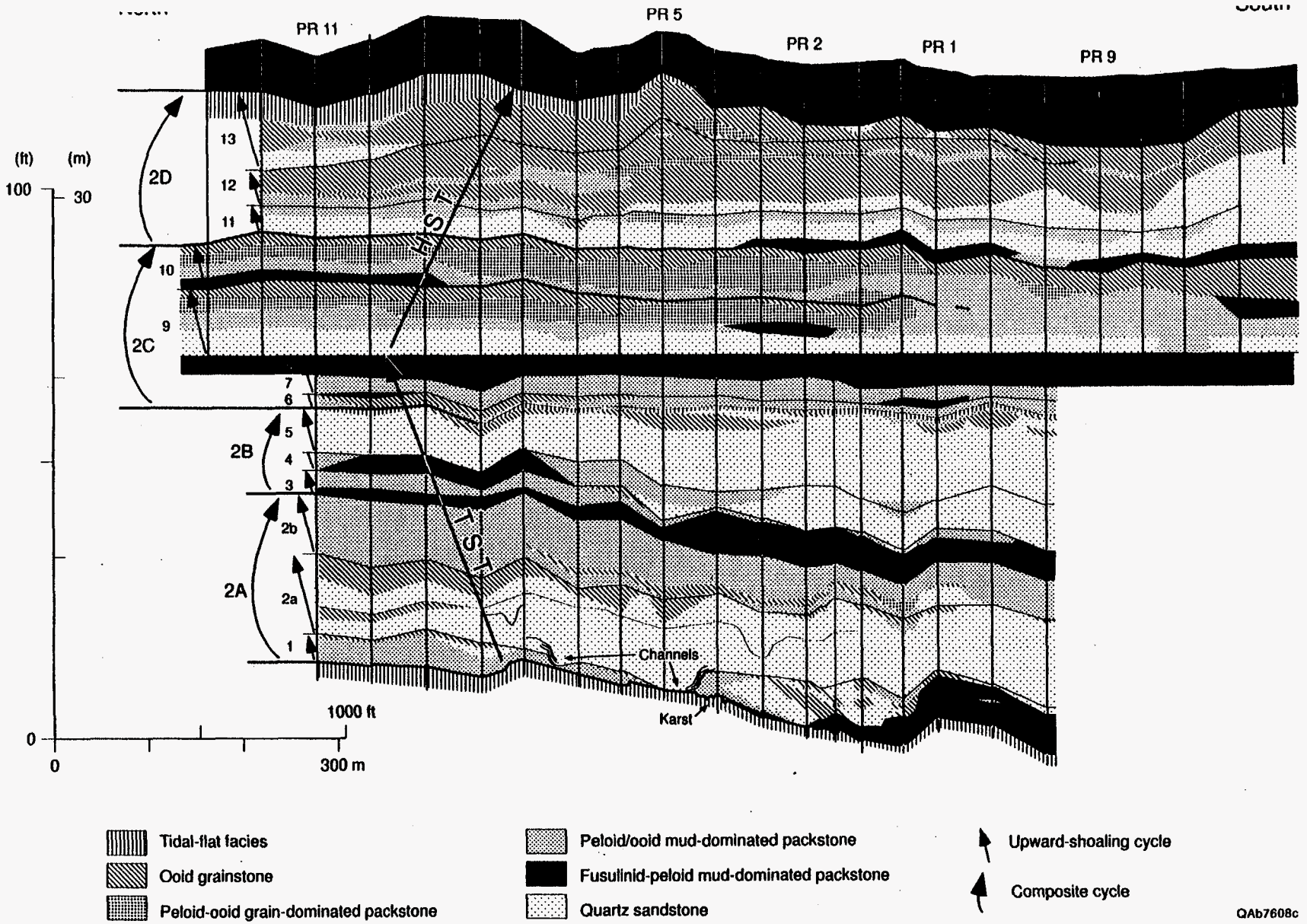

Figure 13. Stratigraphic cross-section of HFS 2 from Plowman Ridge exemplifies the stratigraphic architecture of a Grayburg high-frequency sequence. HFS 2 represents a longer term accommodation trend composed of 14 upward-shoaling cycles. Two or more cycles are organized into intermediate-term transgressive-regressive successions termed composite cycles, four of which (2A–2D) occur in HFS 2.

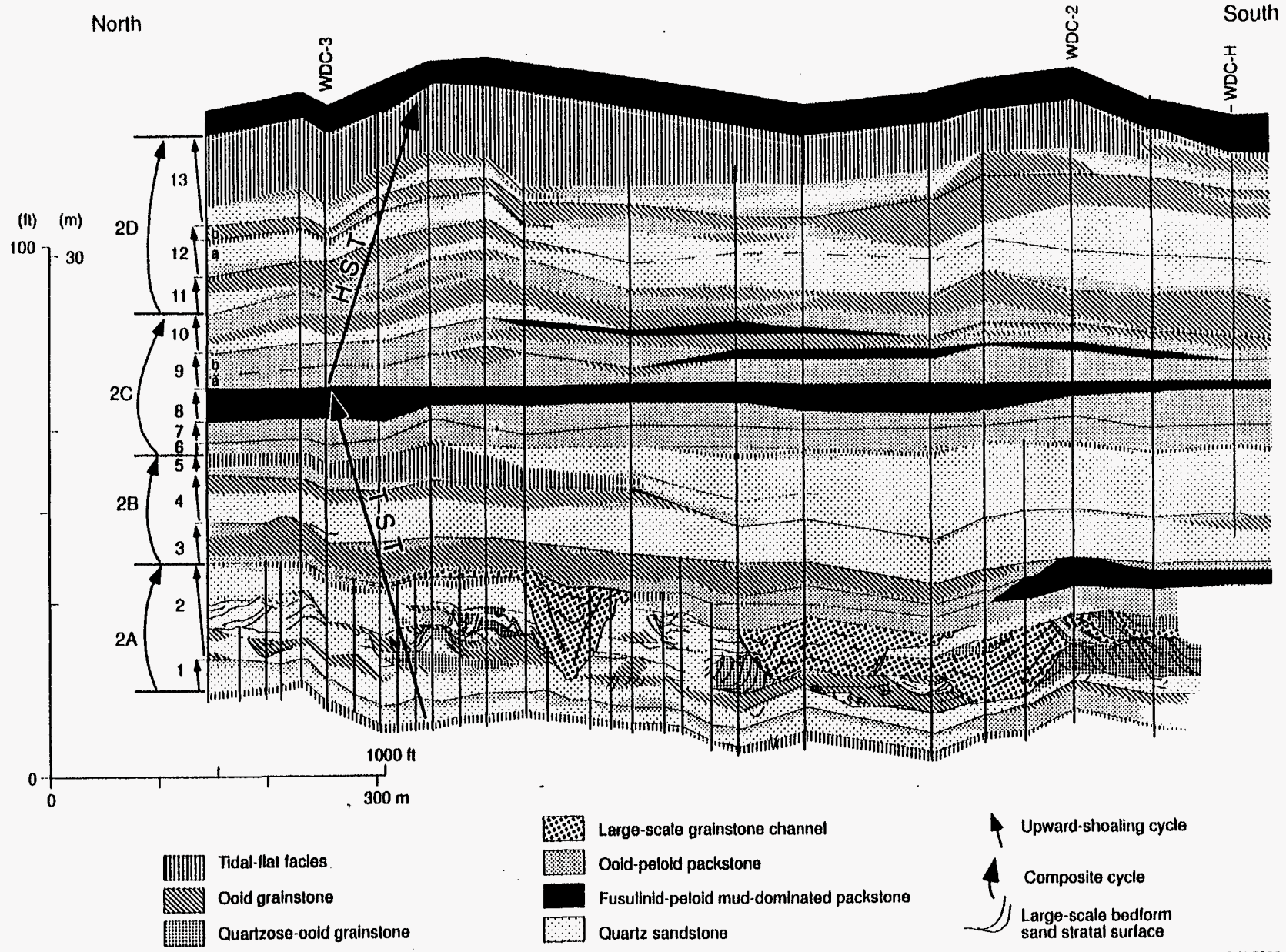

Figure 14. Stratigraphic cross-section of HFS 2 from West Dog Canyon, 0.5 mi across depositional strike from Plowman Ridge and slightly landward of detailed window of HFS 2 from Plowman Ridge (see Fig. 13). Section is [illegible] dip-oriented; however, outcrop exposures along the canyon meanders cause various segments of the cross section [illegible] ion relative to depositional dip. The detailed chronostratigraphic framework permitted cycle-scale correlations b[illegible] ge and West Dog Canyon.

HFS 14 and our Grayburg HFS 3 and 4 are correlative with Guadalupian HFS 15. The Grayburg Formation represents a longer duration (2–4 m.y.) composite sequence, composed of a dominantly transgressive succession (Grayburg HFS 1–2) that culminated in regional flooding at the base of Grayburg HFS 3. This is succeeded by an aggradational highstand succession composed of the remaining portion of Grayburg HFS 3 and all of Grayburg HFS 4. The four high-frequency sequences recognized in the Grayburg by this study correspond to the four high-frequency sequences identified from log and core data of the subsurface Grayburg on the Central Basin Platform (for example, Fig. 15) by Ruppel and Bebout (1995) and Kerans (pers. comm. 1996).

The Grayburg/Queen formational boundary on Shattuck Valley Wall as mapped by Hayes (1964) exhibits local paleokarst features and this unconformity is interpreted to represent a major sequence boundary (Sarg and Lehmann, 1986). Because paleokarst is only locally expressed on the shallow-water platform, however, it cannot be used to regionally define the Grayburg/Queen sequence boundary. This contact is probably inconsistently mapped throughout the area, particularly in areas lacking paleokarst features or with poor outcrop exposure (Kerans and Nance, 1991). Poor exposure of the uppermost Grayburg on Plowman Ridge and in West Dog Canyon made it difficult for us to unequivocally locate the Grayburg/Queen sequence boundary. Near the top of Plowman Ridge, poorly exposed tepee-fenestral facies with grikes filled with dolomitic siltstone (uppermost Grayburg?) are unconformably overlain by recessively weathered, yellow-brown to pink, thin-bedded sandstones that we interpret to represent the lowermost Queen Formation. This stratigraphic relationship was only observed at the southern end of Plowman Ridge, which represents the youngest stratigraphic interval examined by this study.

Sarg and Lehmann (1986) correlated the Grayburg/Queen sequence boundary exposed at Last Chance Canyon, Algerita Escarpment, and Shattuck Valley 10 to 12 mi seaward to the erosional truncation surface on the Western Escarpment described by Fekete and others (1986). This steeply dipping erosional surface truncates at least 650 to 1000 ft of upper Grayburg outer-platform strata and flattens shelfward to merge with flat-lying platform strata. The steeply dipping erosional surface is abruptly overlain by high-angle, sponge-rich foreslope facies of the Goat Seep Dolomite,

which forms the shelf margin to correlative, flat-bedded, shoal-water, carbonates and siliciclastics assigned to the Queen Formation (Fekete and others, 1986; Franseen and others, 1989). Kerans and others (1992a; 1992b; 1993) placed the Grayburg/Queen erosional contact of Fekete and others (1986) and Franseen and others (1989) within the Queen Formation. Both correlations are poorly constrained because of the paucity of detailed mapping and outcrop studies of this bounding surface between the basinward and shelf locations.

DEPOSITIONAL FACIES

Mixed carbonates and siliciclastics of the Grayburg Formation in the Guadalupe and Brokeoff Mountains region represented by the study area (Figs. 7–11) accumulated on a shallow-water platform landward of the terminal margin (Fig. 4). Six major depositional facies are recognized: (1) fusulinid-peloid mud-dominated packstone and wackestone; (2) skeletal-peloid wackestone and mudstone; (3) ooid/peloid mud- to grain-dominated packstone; (4) ooid grainstone; (5) tidal flat facies; and (6) quartz sandstone and mixed quartz sandstone and carbonate lithologies. Although the precursor limestones were replaced by dolomite, sedimentary textures and depositional fabrics are generally well preserved.

Kerans and Nance (1991) established a general facies model for the Grayburg that is superimposed on a dip profile of a ramp with a well developed crest (Fig. 12). The inner-ramp facies tract consists of tidal flat and lagoonal facies. The middle-ramp facies tract is dominated by quiet water massive to burrowed quartz sandstones and higher energy cross-bedded quartz sandstones. The ramp-crest facies tract is dominated by tepee-fenestral facies. The ramp crest grades seaward into crossbedded grainstone shoals that are flanked basinward by successively more distal outer-ramp facies composed of grain-dominated to mud-dominated packstone and wackestone, with locally abundant fusulinids. This model is a good general representation for the Grayburg, except that the lower, dominantly transgressive portion of the Grayburg (HFS 1) did not develop a significant ramp crestal buildup.

Fusulinid-Peloid Mud-Dominated Packstone and Wackestone

Fusulinid-peloid mud-dominated packstones and wackestones are intensively bioturbated to massive units. Abundant (10 to 40 percent) fusulinids define this facies, although it is primarily composed of peloids and carbonate mud. Peloids are ovoid poorly defined grains ranging in size from 60 to 150 microns. Other constituents include mollusks, pelmatozoans, ooids, and quartz sand. Replacement dolomites in this facies form anhedral to subhedral mosaics of aphanocrystalline to finely crystalline dolomite with crystal size generally less than 20 microns, although crystals range up to 60 microns in size.

Fusulinid-peloid mud-dominated packstones and wackestones unconformably overlie high frequency sequence and cycle boundaries. This facies typically occurs at the base of TST cycles (Fig. 8) and is less common in HST cycles. Fusulinid content generally decreases upward within individual facies units.

Fusulinid-peloid mud-dominated packstone and wackestone facies accumulated on the outer ramp (Kerans and Nance, 1991). Reconstructed depositional profiles indicate minimum water depths of 30 ft (Kerans and Fitchen, 1995). Abundant carbonate mud, lack of current lamination, and intense bioturbation affirm a low-energy outer-ramp setting. Because fusulinid-peloid mud-dominated packstone and wackestone facies record maximum water depths on the shallow-water platform, this facies is crucial for stratigraphic interpretations. It records maximum transgression and is also useful to establish chronostratigraphic correlations.

The fusulinid-peloid mud-dominated packstone and wackestone unit at the transgressive base of HFS 3 represents maximum flooding in the Grayburg composite sequence (Kerans and Nance, 1991; Kerans and others, 1992a; 1993; this study). Kerans and others (1992a; 1993) subdivided the Grayburg into two high-frequency sequences (Guadalupian 14 and 15) and assigned this fusulinid-rich unit to the transgressive base of Guadalupian 15. This maximum flooding event also is recognized in the Central Basin Platform subsurface (e.g., Ruppel and Bebout, 1995).

In the relatively shallow-water platform Grayburg succession above the San Andres platform, fusulinids are relatively rare above HFS 3 (this study; Ruppel and Bebout, 1995) because of decreasing long-term accommodation in the Grayburg composite sequence. In strata that accumulated seaward of the San Andres margin, however, fusulinid-rich facies persist throughout the Grayburg up to the Grayburg-Queen sequence boundary (Kerans and Nance, 1991), reflecting greater accommodation in this more basinal succession.

Within the high-frequency sequences, the distribution of fusulinid-peloid mud-dominated packstones and wackestones in successive cycles is a defining aspect of the internal stratigraphic framework. For example, in HFS 2 (Fig. 13), transgression by fusulinid-bearing facies above fenestral dolomites of the underlying HFS 1 defines the lower sequence boundary. The TST records successive transgression by fusulinid-bearing facies, which culminated in deposition of a fusulinid-peloid mud-dominated packstone unit that records maximum flooding in HFS 2. Fusulinids are less common in the HST except at the base of some cycles. At the top of HFS 2, ramp-crest tidal flat and ooid grainstone facies are abruptly overlain by fusulinid-rich facies, recording an abrupt landward facies tract offset that represents the ensuing transgression.

Skeletal-Peloid Wackestone and Mudstone

Carbonate mud and peloids are the major constituents of skeletal-peloid wackestone and mudstone facies. This facies locally displays faint parallel lamination, although intensive bioturbation is more common. Peloids are ovoid, typically poorly defined grains ranging in size from 60 to 150 microns. Because of intense bioturbation, compaction, and dolomitization, peloids locally are difficult to distinguish from carbonate mud matrix. Minor local skeletal debris includes fusulinids, mollusks, pelmatozoans, and rare dasycladaceans. Quartz sand is locally common. True mudstones are rare in the Grayburg interval examined by this study. Replacement dolomites form anhedral to subhedral mosaics of aphanocrystalline to finely crystalline dolomite with crystals generally smaller than 20 microns, although crystals locally range up to 60 microns.

This facies, although relatively uncommon, occurs throughout the Grayburg in both TST and HST settings in inner- to outer-ramp locations. Skeletal-peloid wackestone and mudstone facies typically occur at cycle bases. The abundant carbonate mud, extensive biotic reworking, and the general stratigraphic distribution of this facies indicate a low energy subtidal environment. On the outer ramp this facies accumulated below fair-weather wave base. Extensive biotic reworking attests to low deposition rates. This facies also locally occurs in inner-ramp lagoonal settings protected from high-energy currents by seaward ramp crest shoals.

Ooid/Peloid Packstone Facies

Peloid mud-dominated packstone - Peloid mud-dominated packstones are massive to vertically burrowed units, composed of dominantly peloids and carbonate mud, with local poorly defined parallel lamination. Other constituents include ooids, fusulinids, pelmatozoans, mollusks, and quartz sand. Carbonate mud completely occludes primary interparticle pore space. Replacement dolomites form anhedral to subhedral mosaics. Dolomite crystal size is variable; some fabrics are dominated by aphanocrystalline to finely crystalline dolomite with crystals smaller than 20 microns. Replacement dolomite also forms very finely to finely crystalline fabrics with crystals ranging from 10 to 60 microns in size.

This is an abundant facies in both TST and HST strata. It typically occurs at the base of cycles and grades upward into grain-dominated packstone. Mud-dominated packstone facies typically display poor lateral continuity and grade laterally into fusulinid-peloid mud-dominated packstone, grain-dominated packstone, and quartzose peloidal mud-dominated packstone.

Peloid mud-dominated packstones represent *in situ* pelletization of lime muds by benthic fauna and traction deposition of weakly indurated fecal pellets and peloids by higher energy currents and introduction of carbonate mud by biotic reworking. This records dominantly quiet water deposition below fair-weather wave base on the outer ramp and/or a shallow lagoonal setting protected from high-energy currents by seaward ramp crest grainstone shoals. Successive grain-dominated packstones record aggradation into higher energy, better winnowed environments.

Peloid-ooid grain-dominated packstone - Peloid-ooid grain-dominated grainstone units display local relict parallel- to cross-stratification partially overprinted by bioturbation. Ooids (150 to 500 microns) and peloids (60 to 150 microns) are the dominant grain type; other constituents include carbonate mud, pelmatozoans, mollusks, intraclasts, and quartz sand. Carbonate mud partially occludes primary interparticle pores, which were completely to incompletely filed by carbonate cement. Replacement dolomite forms anhedral to subhedral mosaics of dolomite crystals 10 to 80 microns in size. Micritic grains and carbonate mud locally are replaced by dolomite mosaics that contain aphanocrystalline (less than 4 microns) to 10 micron crystals.

This facies occurs in both TST and HST cycles but is most abundant in the HST. Grain-dominated packstones generally are restricted to the upper portion of depositional cycles and are gradationally to abruptly overlain by ooid grainstones. Grain-dominated packstone facies commonly display poor lateral continuity and grade laterally into mud-dominated packstone and/or into ooid grainstone facies.

Peloid-ooid grain-dominated packstone facies record upward-shoaling into a higher energy setting. Admixture of carbonate mud and destruction of much of the primary stratification were induced by bioturbation. Peloid-ooid grain-dominated packstone facies flanked ooid ramp-crest shoals, which were the focus of active ooid formation and deposition. In the adjacent grain-dominated packstone facies and during depositional hiatuses, lower depositional rates allowed benthic fauna to rework the sediments and introduce admixed carbonate mud.

Ooid Grainstone

Ooid grainstones are cross-stratified units dominated by well-sorted ooids (150 to 500 microns). Carbonate mud is absent and primary interparticle pore space is partially to completely occluded by carbonate cement. Although many ooids display concentric internal laminations, their internal fabrics commonly have been obliterated by dolomitization. Peloids, intraclasts, pelmatozoans, and quartz sand, commonly with ooid-coated rims, are locally abundant. Replacement dolomites form anhedral to subhedral mosaics of 10 to 80 micron dolomite crystals.

Micritic grains often were replaced by more finely crystalline dolomite mosaics that range from aphanocrystalline (less than 4 microns) up to 10 microns.

Ooid grainstones are present in both TST and HST strata. Highstand ooid grainstone bodies, however, are more abundant and exhibit greater lateral continuity than transgressive ooid grainstones (Fig. 9). Upward-shoaling cycles capped by ooid grainstones are most typical of the HST. Ooid grainstones are volumetrically most abundant in the HFS 2 HST, both in the outcrop (Fig. 9) and in the subsurface (Fig. 15).

Ooid grainstone units generally are composed of multiple stacked medium to thick beds of sheet-stratified to small- to medium-scale planar and trough crossbeds of ooid grainstone that are amalgamated into units up to 14 ft thick. These grainstone units locally are interrupted by thin (less than 1 ft thick) intervals of slightly bioturbated ooid grain-dominated packstone, some of which exhibit lateral dip continuity of several hundred feet (Fig. 13). Grainstone shoals grade laterally into flanking ooid grain-dominated and mud-dominated packstones with extensive bioturbation. Other grainstone units display a channel morphology and contain medium- to large-scale trough crossbeds.

Ooid grainstones are stratigraphically critical facies because they are a sensitive indicator of high-energy, shallow-water deposition on the ramp crest and their distribution through successive cycles thus reflects longer-term accommodation trends.

Grainstone Body Heterogeneity - Transgressive ooid grainstones typically are discrete bodies that represent an individual depositional event, such as an episode of tidal-channel filling or lateral bar accretion. These grainstone bodies commonly retained their initial depositional morphologies and were not extensively reworked and amalgamated. Grainstone channels are up to 15 ft thick, with sharp erosional bases that downcut underlying strata. The channels are oriented subparallel to depositional dip (Fig. 16) and are up to several hundred feet wide. Accretionary shoals and bars formed depositional highs. Syndepositional relief is at a maximum in these high-energy channels and shoals, and individual large-scale bedforms have up to 10–15 ft of relief from topset to toeset. Transgressive ooid grainstones are characterized by variable admixtures of ooid grainstone and

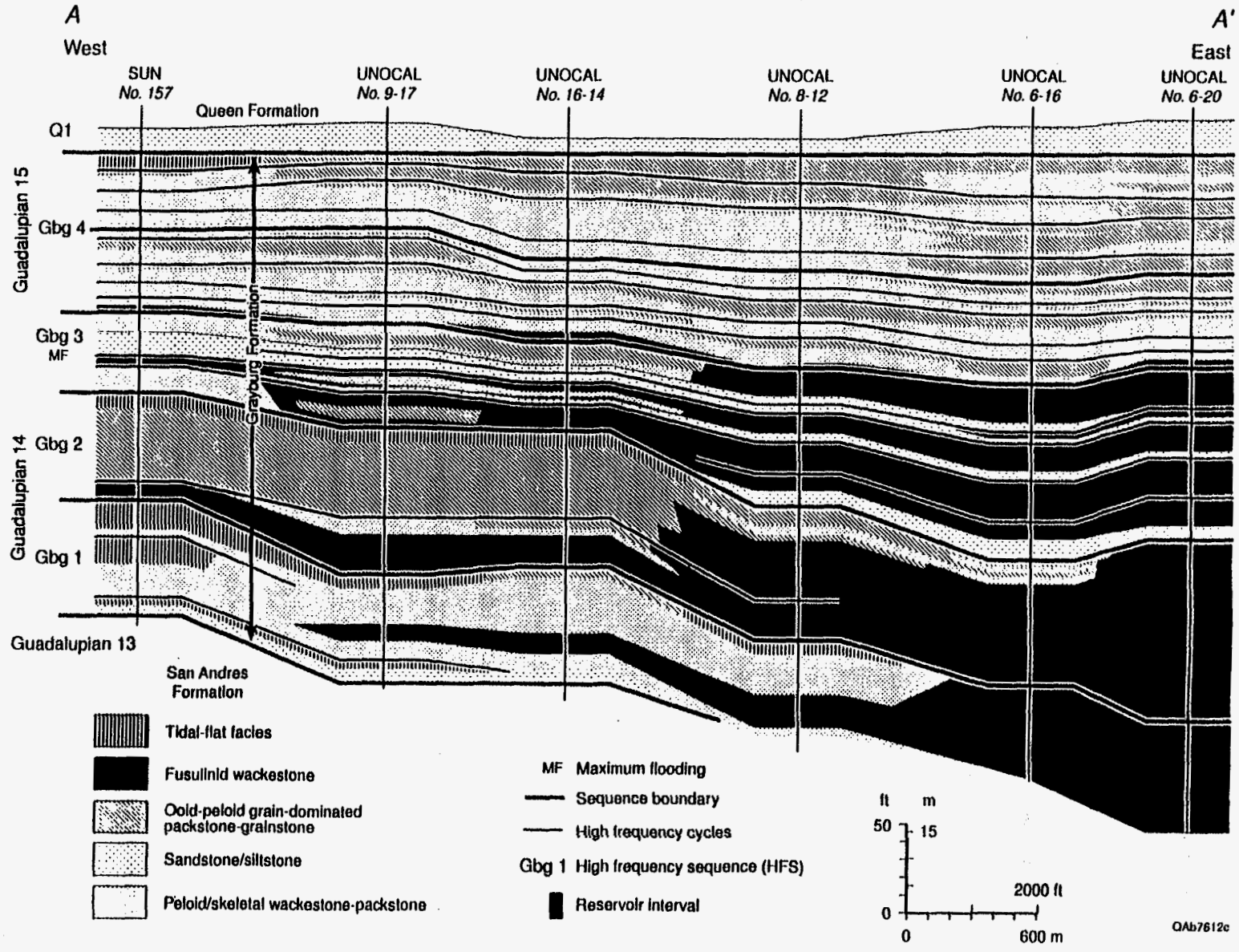

Figure 15. Grayburg stratigraphic framework from South Cowden field from Ruppel and Bebout (1995). Dip-oriented section documents four high-frequency sequences within the long-term accommodation trend of the Grayburg composite sequence. Stratigraphic framework and facies architecture are similar to that of the Grayburg outcrop study (see Fig. 7).

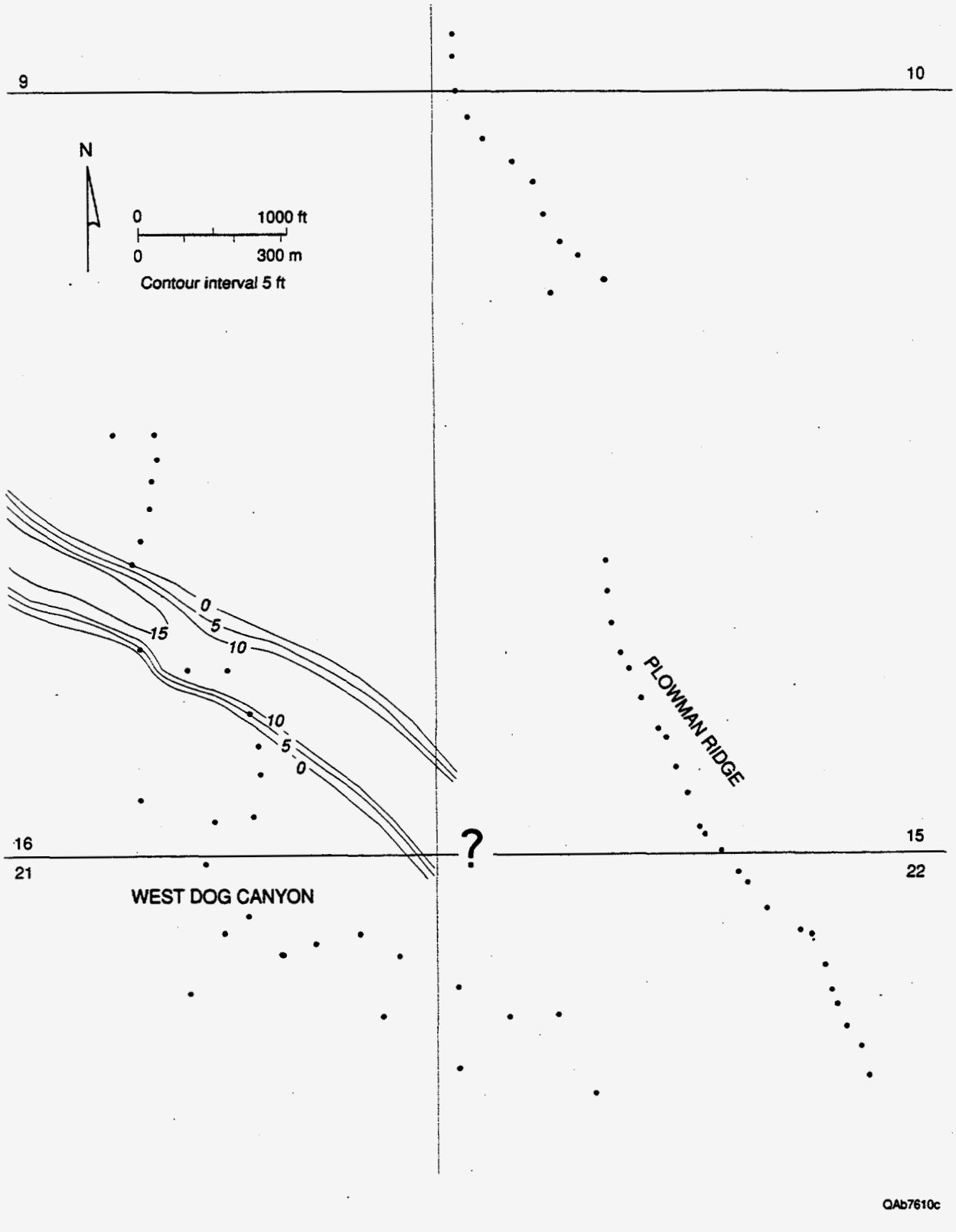

Figure 16. Isopach map of ooid-intraclast grainstone-filled tidal channel in HFS 2 cycle 2. Dots indicate measured sections used to generate map. Township and range lines from figure 5.

quartz sandstone, which reflect open communication between the siliciclastic-dominated inner platform and the ramp crest via tidal channels.

Ooid grainstone bodies in the HST exhibit greater lateral continuity, both along dip (Figs. 13 and 14) and across strike. For example, the isopach map of the grainstone in Grayburg HFS 2 cycle 12 (Fig. 17) shows that this grainstone body forms a strike-elongate shoal. The crest attains a maximum thickness of 14 ft, and is laterally continuous for more than 4,000 ft along dip and at least 3,000 ft across strike. The ooid grainstone body thins landward and grades into peloidal-ooid mud-dominated packstones and dolomitic sandstones. The predominantly south-dipping foresets within these grainstone units suggest that sediment transport was from the north, which may reflect either leeward transport by the prevailing paleowinds or an ebb-tidal dominated setting.

Development of ooid shoals and tidal channels on the ramp crest is comparable to that observed in modern carbonates in the Joulters Cay area of the Bahamas (Harris and others, 1993). The transgressive systems tracts exhibit the greatest lateral heterogeneity of grainstone bodies, many of which formed dip-elongate channels and bars (Fig. 16). This extreme heterogeneity (tens to hundreds of feet) reflects the tidal setting that dominated during initial transgression, in which ooids were produced and accumulated along dip-elongate tidal channels and bars. Rapid increase in accommodation associated with relative sea-level rise resulted in high preservation potential for these grainstone bodies. Transgressive ooid grainstone bodies with poor lateral continuity may also partially reflect the influence of inherited topographic highs on facies distribution. These topographic highs were mantled by sediment during transgression and did not greatly influence facies distribution in the subsequent highstand systems tract.

Limited accommodation in the highstand systems tract resulted in reworking, coalescence and amalgamation of high-energy ramp crest ooid grainstone bodies to form strike-elongate shoals (Fig. 17) that are laterally continuous (thousands of feet) along dip and across strike. These ooid grainstones typically contain little or no admixed quartz sand, suggesting that communication with the siliciclastic-dominated inner platform was inhibited by barrier bars of ooid grainstone. The considerable thickness and lateral continuity of highstand ooid grainstone units may also record

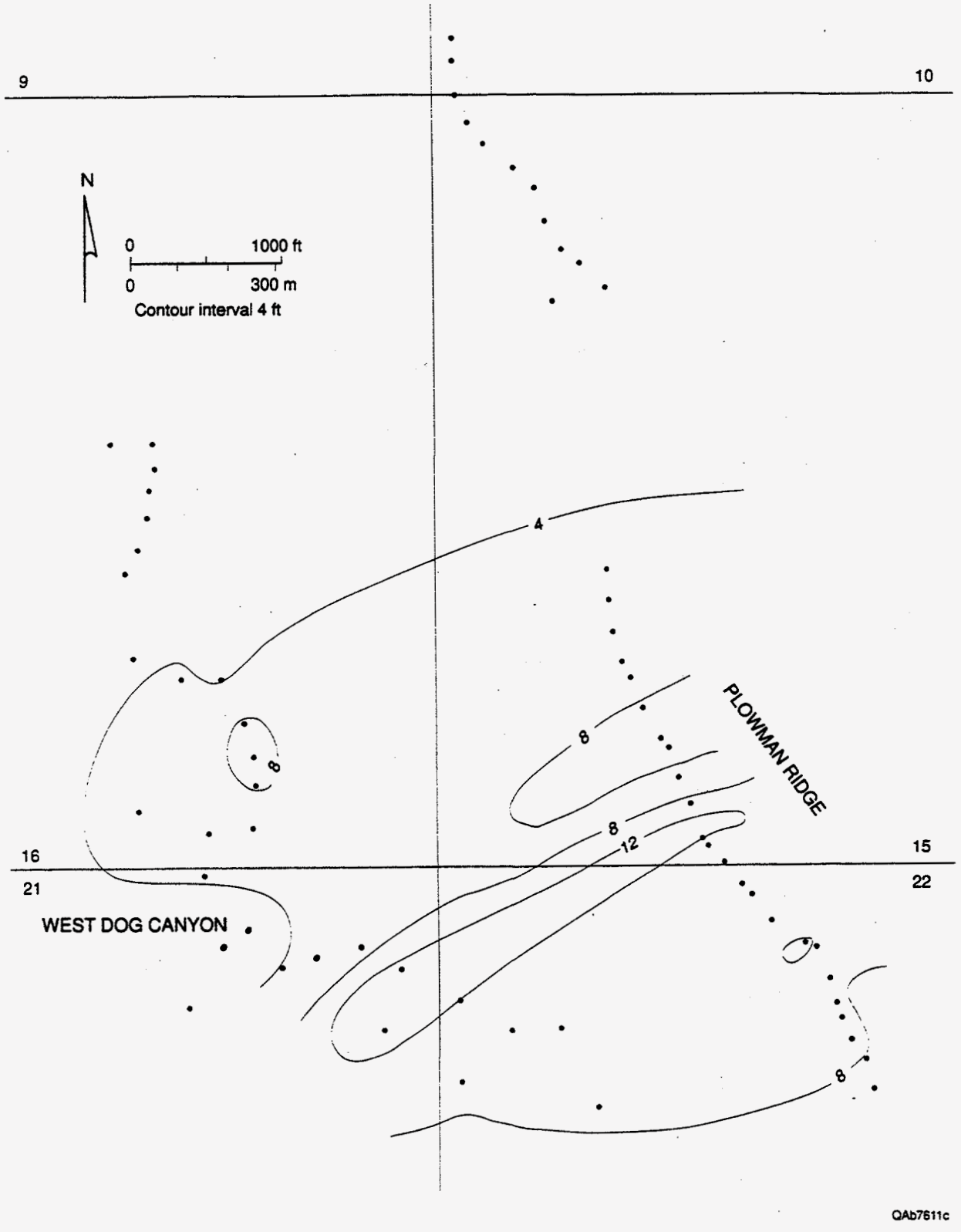

Figure 17. Isopach map of ooid grainstone unit in Grayburg HFS 2 cycle 12. Dots indicate measured sections used to generate map. Township and range lines from figure 5.

unrecognized amalgamation of two or more ooid grainstone-dominated cycles in this low accommodation, wave- to ebb-tidal-dominated, ramp crest setting.

Tidal Flat Facies

Tidal flat facies exhibit tepee-fenestral, algal-laminated, and pisolitic fabrics that record supratidal environments. This facies typically caps cycles near the tops of the high-frequency sequences (Fig. 10). The upper bounding surface of these units commonly is irregular and locally displays erosional truncation and/or small-scale karst dissolution. Fenestral fabrics typically have a gradational base and lowermost fenestrae are diffuse and poorly developed, whereas fenestrae increase in their definition, size, and abundance towards the top of this facies. Tepee fabrics contain abundant fenestrae, pisoids, marine-cemented sheet cracks and internal sediments. Algal laminated facies, including stromatolites, are especially common in inner ramp locations but also are associated with tepee-fenestral fabrics. Desiccation cracks occur throughout this facies and *in situ* breccias are common. Replacement dolomites form anhedral to subhedral mosaics of aphanocrystalline to finely crystalline dolomite ranging from less than 1 to 20 microns in size. Primary fenestral and interparticle pore space is occluded by cement consisting of anhedral dolomite crystals up to 80 microns.

At inner-ramp locations, fenestral and algal-laminated fabrics are associated with carbonate mud-rich tidal flat facies. Inner-ramp tidal flat facies locally contain admixed quartz sand and commonly grade laterally into dolomitic sandstones that also display tidal flat fabrics. The best developed and thickest pisolitic tepee-fenestral fabrics occur within grainstone and packstone precursor facies at the ramp crest. At this locale, pisolitic tepee-fenestral fabrics are interbedded with minor subtidal grainstone and packstone beds. Marine cements, including originally aragonitic botryoids, line the roofs of sheet cracks and internal sediments form geopetal floors.

Tepee-fenestral and algal-laminated facies record episodic exposure in supratidal environments. At inner-ramp locations, these facies represent *in situ* accumulation on prograding tidal flats as well as diagenetic overprinting by tepee-fenestral-pisolitic fabrics on carbonate mud-

rich lagoonal facies during supratidal exposure. Admixed quartz sand reflects eolian deposition on tidal flats and subsequent reworking during storms. On the ramp crest, thick accumulations of pisolitic tepee-fenestral facies record carbonate grain-rich precursor facies that aggraded to above sea level and were subsequently diagenetically overprinted by vadose processes in a supratidal environment. Interbedded subtidal grainstone and packstone beds attest to the proximity of the ramp crest to flanking subtidal facies and episodic storm deposition. Abundant sheet cracks, botryoidal marine cements, geopetal sediments, and pisoids in the ramp crest tepee-fenestral facies indicate vadose diagenesis by marine waters.

Tidal flat facies are stratigraphically significant as they record platform aggradation to sea level and above. This facies association is crucial for determining the sea level cyclicity and establishing high-frequency stratigraphic sequences. This facies type is best developed at the tops of the high-frequency sequences (Fig. 10), which is also true for the subsurface Grayburg in South Cowden field (Fig. 15). The tops of tidal flat facies locally display erosional truncation and small-scale karst, indicating subaerial exposure. Where these unconformable surfaces are abruptly overlain by outer-ramp fusulinid-peloid mud-dominated packstone and wackestone facies, this landward facies tract offset records an ensuing transgression. These stratal relationships were used to help delineate the high-frequency sequence boundaries (Fig. 7).

Quartz Sandstone and Mixed Siliciclastic-Carbonate Facies

Siliciclastics in the Grayburg are represented by white to dark brown quartz sandstones that form prominent marker units that can be traced laterally along outcrop exposures in the Brokeoff Mountains region. Sandstones consist of very fine- to medium-size quartz sand grains, minor feldspar grains, and variable admixtures of dolomitized carbonate material. Sand grains in the very fine- and fine-size fractions are angular, whereas the medium sand grains are rounded to well-rounded. Siliciclastic silts or clays are absent.

Quartz sandstone and mixed siliciclastic-carbonate lithologies occur throughout the Grayburg composite sequence (Fig. 11), although the lowermost Grayburg (HFS 1) has the greatest

abundance of siliciclastics. Quartz sandstone occurs in both transgressive and highstand strata. Quartz sandstone is least abundant in cycles associated with maximum flooding of the platform. In mixed siliciclastic-carbonate cycles, quartz sandstone typically occurs at the cycle base.

Mixed siliciclastic-carbonate lithologies occur locally in all of the major carbonate facies. Siliciclastic-carbonate admixtures display a continuum from less than 5 percent to nearly 100 percent quartz sand. In the field it can be difficult to accurately estimate the quartz sand content, because quartz sand is overemphasized on weathered surfaces. Moreover, quartz sand abundance commonly displays considerable vertical and lateral variation at all scales. These factors make consistent delineation and mapping of these mixed lithology rocks extremely difficult.

Quartz sandstones, as designated in this study, contain more than 60–70 percent quartz sand, and their carbonate content and facies were used to modify their description. Rocks containing approximately subequal amounts of quartz sand and carbonate are the most difficult to classify consistently. Such rocks were designated as 'dolomitic quartz sandstone' or 'quartzose dolomite.' Mixed siliciclastic-carbonate rocks containing less than 40 percent quartz sand were classified according to their major carbonate facies (see above), and quartz sand content was used as a modifier. Quartz sandstones were subdivided into three major facies: (1) massive quartz sandstone; (2) cross-stratified quartz sandstone; and (3) tidal flat quartz sandstone.

Massive quartz sandstone - This facies is thick-bedded and is massive to vertically burrowed. It contains up to 40 percent dolomitized carbonate, dominantly fusulinids, peloids, intraclasts, and carbonate mud. This facies occurs at the base of cycles and reflects a low energy subtidal setting on the inner to middle ramp.

Cross-stratified quartz sandstone - This facies is composed of thin- to medium-bedded sandstone units that exhibit minor burrowing and is dominated by current stratification, including small- to medium-scale trough cross-beds, low angle cross-stratification, and ripple lamination. This facies contains up to 40 percent dolomitized carbonate, including fusulinids, peloids, ooids, and intraclasts. Carbonate mud is absent. This facies occurs in the upper portion of cycles, above basal massive to burrowed sandstones and locally persists to the cycle tops, or it may be overlain

by mixed siliciclastic-carbonates, carbonates, or tidal-flat quartz sandstone. This facies records a high-energy subtidal setting dominated by tidal- and wave-induced currents.

Tidal flat quartz sandstone - This facies consists of thin- to medium-bedded sandstone units with tidal flat fabrics, including wavy to crenulated algal-bound lamination, stromatolites, fenestrae, desiccation cracks, and breccia beds composed of carbonate clasts within a sandstone matrix. These tidal flat sandstones contain up to 40 percent dolomitized carbonate, including pisoids, ooids, peloids, intraclasts, and carbonate mud. Fossil fragments and burrows are rare to absent. This facies records inner ramp quartz sand-rich tidal flat environments.

The size distribution of the quartz sand grains, the well-rounded morphology of medium-size quartz sand grains, the mineralogical maturity, and the excellent sorting implies that they were transported by eolian processes. Fischer and Sarnthein (1988) interpreted that siliciclastics in the Permian Basin region reflect widespread continental exposure during sea level lowstands, which resulted in eolian transport of quartz sand to the outer platform by prograding eolian dunes, and that finer silt-size siliciclastics bypassed the platform and accumulated in the basin. Paleolatitude and paleogeographic reconstructions place the Delaware and Midland Basins region slightly north of the equator during the upper Permian, rotated approximately 40 degrees east of present day north (see Walker and others, 1995). This location in the southern portion of the trade wind belt implies that prevailing winds were from the paleo-northeast, near present-day north (Fischer and Sarnthein, 1988; Walker and others, 1995). Consequently, abundant quartz sand in shallow-water platform Grayburg strata records widespread exposure during sea level lowstands and concomitant progradation of eolian dunes to the outer platform by prevailing trade winds. During the ensuing transgressions, eolian-deposited quartz sands were reworked in a subtidal environment, as attested by admixed skeletal grains, including fusulinids, mollusks, and pelmatozoans and by locally intensive bioturbation.

Quartz sandstones and mixed siliciclastic-carbonate lithologies are stratigraphically significant, because they record widespread exposure during cyclic falls in relative sea level. The occurrence of quartz sandstone in both transgressive and highstand strata implies that sea level lowstands resulted

in widespread exposure of the platform during both initial transgression and as the platform aggraded to sea level during the late highstand. Quartz sandstone is least abundant in cycles associated with maximum flooding when sand influx was limited.

Other Facies

The lower transgressive portion of the Grayburg (HFS 1 and the lower portion of HFS 2) is composed of a complex facies assemblage of tidal channels and interchannel sand ridges. These facies bodies are dip elongate. Large-scale trough cross bedding is abundant, and erosional truncation is common. Large-scale channels downcut up to 16 ft into underlying strata. These facies contain highly variable admixtures of ooids and quartz sand. Channel-fill deposits locally consist of coarse intraclast gravel and intraclast-ooid grainstone. Skeletal material generally is not abundant, but fusulinids, pelmatozoans and mollusks occur locally. Rare burrows in these tidal channels and ridges are typically large (>1 inch diameter) horizontal burrows with backfilled structures, which appear to have formed immediately below the depositional surface.

These facies represent a high-energy shallow water setting prevalent during initial transgression. A tidal-dominated setting is indicated by sedimentary structures and the dip orientation of facies bodies. Mixed carbonate-siliciclastic facies attest to open communication between siliciclastic-dominated inner ramp and the ooid-dominated outer ramp via tidal channels.

STRATIGRAPHIC HIERARCHY

The Grayburg composite sequence represents a long-term (2–4 m.y.) accommodation cycle (Sarg and Lehmann, 1986; Kerans and Nance, 1991). This study subdivides the Grayburg composite sequence into four high-frequency sequences (Fig. 7). In general, HFS 1 and 2 record increased accommodation during long-term transgression, the base of HFS 3 represents maximum flooding, and the remaining portion of HFS 3 and all of HFS 4 reflect decreased accommodation during late highstand. A similar stratigraphic organization (Fig. 15) is recognized in equivalent Grayburg reservoirs on the Central Basin Platform (Ruppel and Bebout, 1995; Kerans, pers.

comm. 1995). The high-frequency sequences each contain multiple composite cycles (15–40 ft thick), which are smaller-scale transgressive-regressive successions that contain two or more genetically related cycles. Cycles (3–30 ft thick) represent the smallest-scale, upward-shoaling vertical facies successions that can be correlated along the platform-to-basin profile across various facies tracts and constitute the basic chronostratigraphic units for high-resolution correlation.

The three levels of stratigraphic hierarchy (cycles, composite cycles, and high-frequency sequences) within the Grayburg composite sequence are defined from a dip-oriented cross-section by: (1) transgressive-regressive relationships; (2) vertical stacking patterns and lateral facies progressions; (3) abrupt vertical facies tract offsets; and (4) lateral tracing of unconformable stratal surfaces. This stratigraphic organization cannot be adequately defined using vertical facies successions or cycle stacking patterns from an individual vertical section at one location along the platform-to-basin profile. Moreover, the significance of many stratal surfaces cannot be determined from a single vertical section, but rather it is the lateral continuity and variable expression of these stratal surfaces across different facies tracts that define their relative importance. After this stratigraphic relationships and hierarchy are defined for an area, however, they can be readily recognized in additional sections, which can then be correlated into the stratigraphic framework.

Cycles

Cycles are 3 to 30 ft thick and are defined by repetitive, upward-shoaling facies successions. In low accommodation shallow-water carbonate platforms such as the Grayburg, most cycles are asymmetric and record successively shallow water environments as the platform aggraded to sea level. Stratal surfaces at the tops of most cycles are sharp, recording a period of subaerial exposure and/or nondeposition following cycle deposition. Rare, partially symmetric cycles preserve the initial transgressive portion of the ensuing cycle and thus record the "turn-around" from upward-shoaling to upward-deepening conditions.

Cycles form the fundamental chronostratigraphic unit for high-resolution correlation, mapping of facies heterogeneity, and facies interpretation (Kerans and others, 1994). Cycles defined by this

study were correlated throughout the area by physically walking out cycle tops and by tracing stratal relationships on outcrop photographs of laterally continuous strata on Plowman Ridge and in West Dog Canyon. Upward-shoaling vertical facies successions that were not laterally continuous were considered to reflect autocyclic processes such as shoal accretion, washover-fan progradation, and tidal channel filling and migration.

Cycles typically contain a basal transgressive unit of low energy, generally bioturbated facies that record an abrupt increase in water depth. Poorly sorted basal facies are succeeded by more grain-rich lithologies, reflecting increased winnowing by wave and current energy as sediment began to fill accommodation. Quartz sandstone and peloid-ooid grainstone facies with tabular- and trough- cross stratification, ripple lamination and sheet stratification attest to shallowing into a high-energy subtidal setting above fair weather wave base. Fully aggraded cycles are capped by tidal flats, recording shallowing to supratidal environments and complete filling of accommodation space. Grayburg cycles in the study area, however, did not generally fill available accommodation and typically are capped by subtidal facies. Therefore, in many cases, the landward facies offset above the cycle defines the cycle top. A few cycles are capped by subaerial exposure features, including small-scale paleokarst, sand-filled grikes, *in situ* breccias, and desiccation cracks.

Grayburg cycles are composed of quartz sandstone, dolomite, and admixtures of both (Fig. 18). These different cycle types reflect various factors, including the platform location and facies tract, along with their relation with longer-term accommodation trends imposed by the Grayburg composite sequence and the high-frequency sequences.

Some cycles were not recognized due to amalgamation, and unusually thick 'cycles' likely represent amalgamation of two or more cycles. Preservation potential of individual cycles in a shallow-water platform environment reflects various factors, including longer term accommodation trends, constituent facies, and depositional setting. Cycles composed entirely of quartz sandstone are less likely be preserved than carbonate cycles, because carbonates are more likely to be indurated by early cementation and to be preserved. Cycles composed of dominantly high-energy tidal channel or shoal facies are more likely to have been erosionally reworked during deposition of

CYCLE EXAMPLE	LITHOLOGY	COMMON VARIATIONS WITHIN OTHER CYCLES	INTERPRETATION
SANDSTONE-DOMINATED CYCLE			
(a) 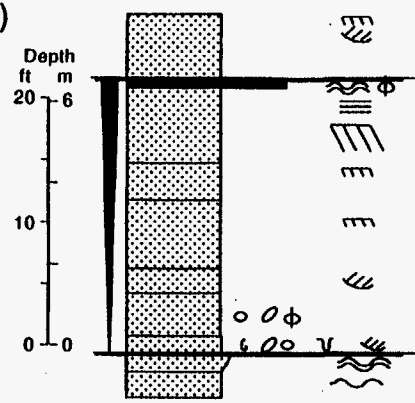	Cross-stratified quartz sandstone		
	Tidal-flat dolomite with algal lamination Planar-stratified quartz sandstone Cross-stratified quartz sandstone	Algal laminite cap may not be present or may be algal laminated quartz sandstone, fenestral quartz sandstone, or dolomite	*Aggradation to sea level* Supratidal deposition and algal binding
	Cross-stratified quartz sandstone Trough-cross-stratified quartz sandstone		*Aggradation to shoal water* Shoal water dominated by high-energy wind and tidal currents
	Massive skeletal rich quartz sandstone Burrowed quartz sandstone with skeletal rich	Base may be skeletal-peloidal wackestone/mud-dominated packstone	*Transgression* Eolian-deposited quartz sand reworked in low-energy subtidal environment
	Tidal-flat quartz sandstone, algal laminated		
MIXED CARBONATE-SANDSTONE CYCLE			
(b) 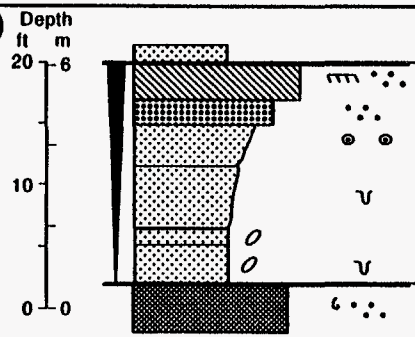	Massive quartz sandstone		
	Cross-stratified ooid grainstone Quartzose pel-ooid grain-dominated packstone Massive dolomitic quartz sandstone with peloids Burrowed quartz sandstone Burrowed quartz sandstone with fusulinids	May be capped by fenestral tidal-flat facies Massive sandstone commonly grades into cross-stratified quartz sandstone	*Aggradation to shoal water* Shoal water dominated by high-energy wind and tidal currents *Transgression* Eolian-deposited quartz sand reworked in open-marine subtidal environment
	Fusulinid-peloid mud-dominated packstone		
CARBONATE-DOMINATED CYCLE			
(c) 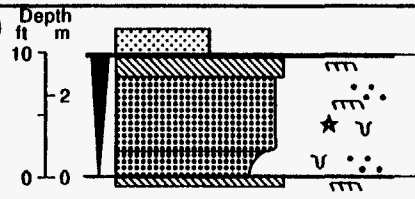	Massive quartz sandstone		
	Cross-stratified ooid grainstone Pel-ooid grain-dominated packstone Burrowed quartzose peloidal mud-dominated packstone	May be capped by fenestral tidal-flat facies Base may be fusulinid mud-dominated packstone or skeletal wackestone	*Aggradation to shoal water* Shoal water dominated by high-energy wind and tidal currents *Transgression* Low-energy subtidal environment
	Cross-stratified ooid grainstone		

QAa8882(a)c

Figure 18. Examples of end-member cycle types developed in the Grayburg Formation.

the following cycle. Lastly, cyclicity in outer ramp facies may be poorly developed, because deeper water facies are relatively insensitive to small-scale cyclic variations in sea level.

Siliciclastic-dominated cycles - The basal portion of siliciclastic-dominated cycles (Fig. 18a) typically is composed of thick-bedded, massive to burrowed quartz sandstone, which contains admixed carbonate, including peloids, carbonate mud, with local fusulinids and other skeletal material. Basal sandstones grade upward into cross-stratified quartz sandstone, which typically displays trough and low angle cross-stratification gradationally overlain by ripple-laminated quartz sandstone. Some siliciclastic-dominated cycles are capped by tidal flat quartz sandstones. Desiccation cracks, breccias, and erosional truncation features occur locally at cycle tops.

Thick-bedded massive to burrowed quartz sandstones with admixed carbonate and fusulinids record reworking of eolian-transported quartz sands in a low energy subtidal setting (Fischer and Sarnthein, 1988). Overlying cross-stratified sandstones indicate aggradation into higher-energy shoal water environments. Aggradation to tidal flat environments is evidenced by wavy to crenulated laminated sandstones that reflect intermittent binding by algal mats and by fenestrae and pisoids. Desiccation cracks, breccia beds, and erosional surfaces capping some cycles attest to subaerial exposure. Some sandstone-dominated cycles, however, do not exhibit a well-defined upward shoaling succession. The caps of some of these cycles are inferred by stratal surfaces with abundant *Thalassinoides*-type burrows, indicating a depositional hiatus, or by overlying abrupt landward facies tract offsets.

Mixed carbonate-siliciclastic cycles - These cycles (Fig. 18b) typically contain a thick-bedded basal unit of massive to burrowed dolomitic quartz sandstone with local fusulinids. Basal dolomitic sandstone grades upward into cross-stratified dolomitic sandstone with increasingly abundant admixed carbonate grains, particularly peloids and ooids. In these mixed lithologic cycles, carbonate content increases upward. In the upper portions of these cycles, dolomitic sandstones are transitionally to abruptly overlain by quartzose peloid-ooid grain-dominated packstones and grainstones. Mixed lithology cycles generally are capped by quartzose grain-dominated packstones and grainstones. Less commonly, mixed carbonate-siliciclastic cycles are capped by tidal flat

facies, dominantly algal-pisolitic-fenestral quartzose dolomites with intraclasts and pisoids. Cycle tops locally display small-scale karst, grikes, and erosional truncation.

In mixed quartz sandstone-carbonate cycles, carbonates become increasingly dominant towards the cycle top as clastic influx diminished during continued rise in relative sea level and *in situ* carbonate production contributed increasingly more sediment. Most mixed carbonate-siliciclastic cycles are capped by high-energy grain-dominated packstones and grainstones, whereas a few cycles fully aggraded to sea level and are capped by tidal flat facies. Rare small-scale karst, grikes, and erosional surfaces record subaerial exposure following cycle deposition.

Carbonate-dominated cycles - These cycles (Fig. 18c) contain basal wackestones and mud-dominated packstones that are intensely bioturbated. Fusulinids, mollusks, and pelmatozoans locally are abundant. These burrowed skeletal-rich facies grade upward into better sorted, peloid-ooid grain-dominated packstones. Burrowing generally decreases upward, and current stratification becomes increasingly dominant. Peloid-ooid packstones are transitionally to abruptly overlain by ooid grainstones. Fully aggraded cycles are capped by tidal flat facies.

Basal skeletal-peloid wackestones and mud-dominated packstones in these cycles record a low-energy, subtidal setting. Fusulinids and pelmatozoans attest to an open marine environment. Carbonate mud content decreases upward, recording increasingly higher energy subtidal environments as the cycle aggraded. The transition from peloid-ooid grain-dominated packstone to overlying grainstones reflects increasingly higher energy deposition. Fully aggraded tidal flat-capped cycles indicate supratidal environments; local subaerial exposure is evidenced by minor small-scale karst and erosional surfaces.

Composite Cycles

Composite cycles (15–40 ft thick) consist of 2 or more cycles that form intermediate-scale transgressive-regressive packages within the longer term accommodation trend imposed by the high-frequency sequence (Figs. 13 and 14). At the base of each composite cycle, transgressive facies of the lowermost cycle typically consist of fusulinid-bearing peloid mud-dominated

packstone and massive quartz sandstone facies. This transgressive facies defines both the base of this cycle as well as that of the larger composite cycle. The magnitude of the facies tract offset recorded by basal transgressive facies of each cycle set is greater than is typical for most cycles.

Cycles in the upper portion of composite cycles contain increasing proportions of shoal-water facies due to successive filling of accommodation. Capping facies, including tidal flats, ooid shoals, and tidal channels (Figs. 13 and 14) record aggradation to high-energy subtidal or supratidal environments. Rare small-scale karst, desiccation cracks, and erosional truncation at the top of some composite cycles evidence subaerial exposure following aggradation to sea level. For many composite cycles, the landward facies tract offset at the transgressive base of the overlying composite cycle is the defining aspect of the composite cycle top. This landward facies tract offset is greater in magnitude than that for most cycles.

Composite cycles subdivide the high-frequency sequences into intermediate-scale transgressive-regressive packages. In the subsurface where well logs and/or cores typically are widely spaced, it can be difficult to identify and correlate individual cycles whereas composite cycles may be more readily recognized and provide chronostratigraphic units that can be confidently correlated. Composite cycles also are useful chronostratigraphic markers in cases where cycle amalgamation has occurred. Amalgamation is restricted to cycles within a composite cycle and cycle amalgamation does not occur across composite cycle boundaries, retaining the integrity of these chronostratigraphic surfaces. Moreover, in cases where cycles are poorly developed and difficult to recognize, such as outer ramp cycles, composite cycles may offer the best opportunity to identify and correlate chronostratigraphic units.

High-Frequency Sequences

The four high-frequency sequences in the Grayburg represent shorter-duration sea level cyclicity superimposed on the long-term (2–4 m.y.) accommodation trend recorded by the Grayburg composite sequence (Fig. 7). The Grayburg high-frequency sequences do not display diagnostic stratal terminations (e.g., onlap, offlap, and toplap) because these relationships did not

develop because of limited accommodation on the relatively flat-lying shallow-water platform. The transgressive systems tract of each high-frequency sequence records a relative rise in sea level that culminated in maximum flooding and widespread deposition of outer ramp facies. The maximum flooding event is succeeded by aggradational and progradational strata of the highstand systems tract. Filling of accommodation during late highstand conditions resulted in widespread deposition of tidal flat facies, followed by subaerial exposure and unconformity development during the ensuing sea level lowstand. The sequence boundary was subsequently transgressed by landward-stepping facies during transgression of the overlying high-frequency sequence.

Sequence boundaries are expressed variably along a dip-oriented platform profile across various facies tracts, across even distances of a few hundred feet (for example, see Fig. 13). Although these unconformable surfaces locally exhibit small-scale karst, grikes, and erosional truncation, subaerial exposure features also locally cap cycles and cycle sets that do not represent sequence boundaries. A major abrupt landward facies tract offset that is laterally persistent across different facies tracts is one of the more diagnostic features of the sequence boundary surfaces (Fig. 7).

Grayburg HFS 1 - Grayburg HFS 1 unconformably overlies the San Andres Formation (Fig. 7) and consists largely of shallow water carbonates and sandstones that record initial flooding of the exposed San Andres platform. The TST contains cycles dominated by quartz sandstone. The lowermost TST cycles contain subtidal quartz sandstones capped by subaerial exposure features, including *in situ* breccias, small-scale karst, and grikes that suggest the incompletely aggraded cycles were stranded by cyclic falls in relative sea level. These cycles are overlain by quartz sandstone-dominated TST cycles with tidal flat caps, indicating that cycles eventually aggraded to supratidal environments.

The first widespread carbonate-dominated cycle in HFS 1, composed of ooid-peloid wackestone to mud-dominated packstone, is interpreted to represent maximum flooding (Fig. 7). This is because it is siliciclastic-poor, suggesting that widespread flooding restricted siliciclastic influx and *in situ* carbonate production dominated sedimentation. Cycles in the HST are more

carbonate-rich than TST cycles. The top of HFS 1 is a widespread tidal flat unit. Rare small-scale karst, grikes, and erosional truncation along the upper bounding surface attest to subaerial exposure.

The isopach map for HFS 1 (Fig. 19) displays a basinward increase in accommodation due to depositional relief on the seaward-dipping top of the San Andres platform (Fig. 7). In the study area, this antecedent topography was essentially filled by the end of HFS 1, as evidenced by widespread tidal flat facies at the top of HFS 1 that record complete platform aggradation.

Grayburg HFS 2 - The basal cycle of HFS 2 (Fig. 7) is a fusulinid-peloid mud-dominated packstone to fusulinid-bearing dolomitic sandstone unit. This records initial flooding of the top of HFS 1 and represents an abrupt landward shift in facies tracts. Tidal currents dominated TST deposition. Continued transgression culminated in deposition of a widespread fusulinid-peloid mud-dominated packstone that records maximum flooding in HFS 2.

Highstand cycles with grain-dominated packstone and grainstone caps record aggradation to a high-energy, wave-dominated subtidal environment due to decreased accommodation during late highstand. The top of the uppermost cycle in HFS 2 is a laterally continuous tidal flat succession that represents complete aggradation and infilling of accommodation. Tidal flat facies at the top of HFS 2 are capped by an unconformable surface with local erosional truncation. This unconformable surface is abruptly transgressed by an outer ramp fusulinid-peloid packstone and wackestone unit.

Because antecedent relief on the San Andres platform was largely infilled by the end of HFS 1, the thickness of HFS 2 displays less pronounced basinward increase in accommodation (Fig. 20). Syndepositional relief in this interval chiefly reflects depositional processes such as sediment production and accumulation on the high-energy outer platform that formed the ramp crest.

Grayburg HFS 3 - Grayburg HFS 3 contains a basal fusulinid-peloid packstone and wackestone unit that records greatest accommodation in the Grayburg composite sequence and maximum regional flooding (Fig. 7). This transgressive unit is recognized throughout the Permian Basin in outcrop and in the subsurface. In the study area, HST cycles of HFS 3 are dominantly

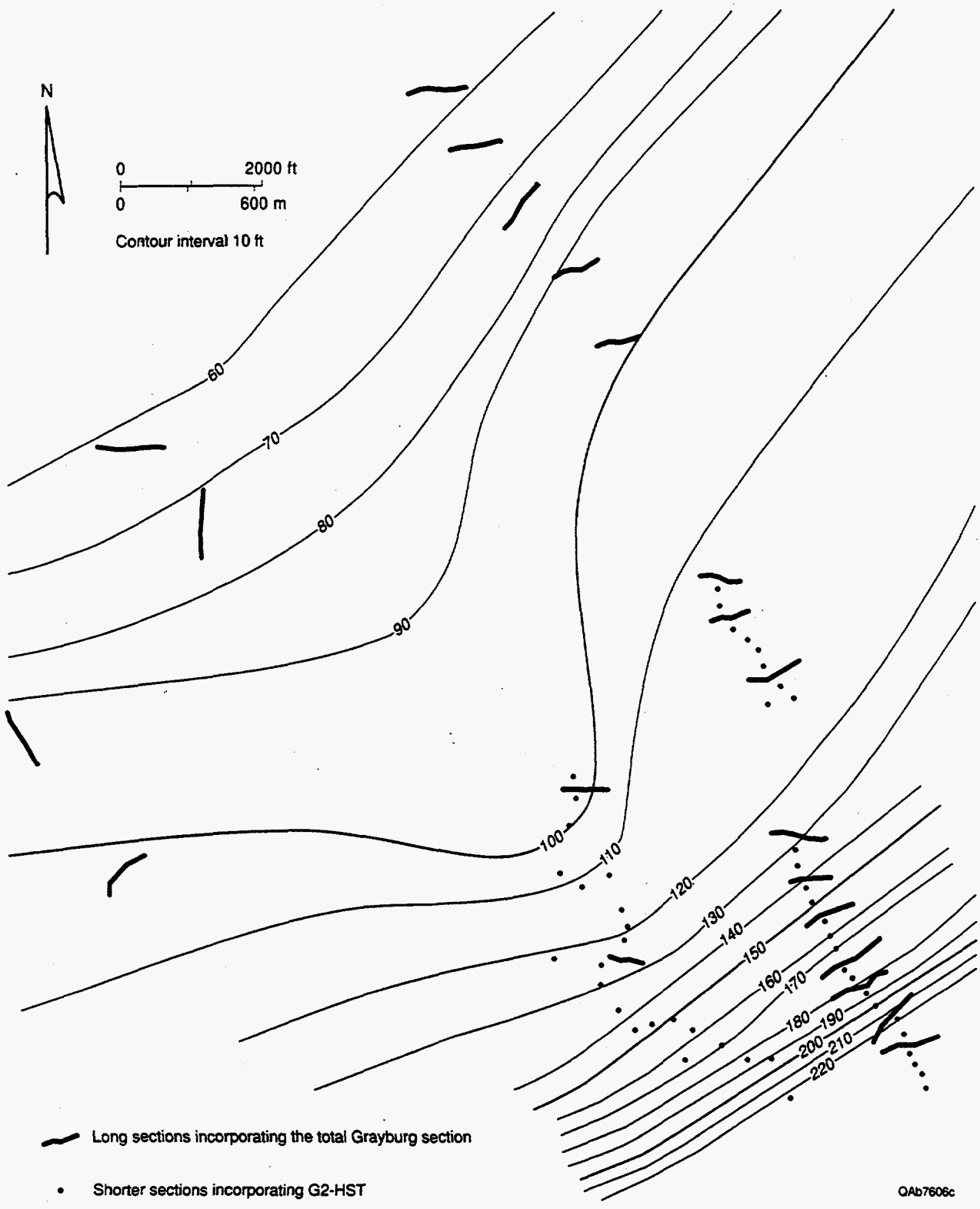

Figure 19. Isopach map of HFS 1 shows influence of antecedent topography on the seaward-dipping top of the underlying San Andres Formation. Most of this differential accommodation was infilled during deposition of HFS 1.

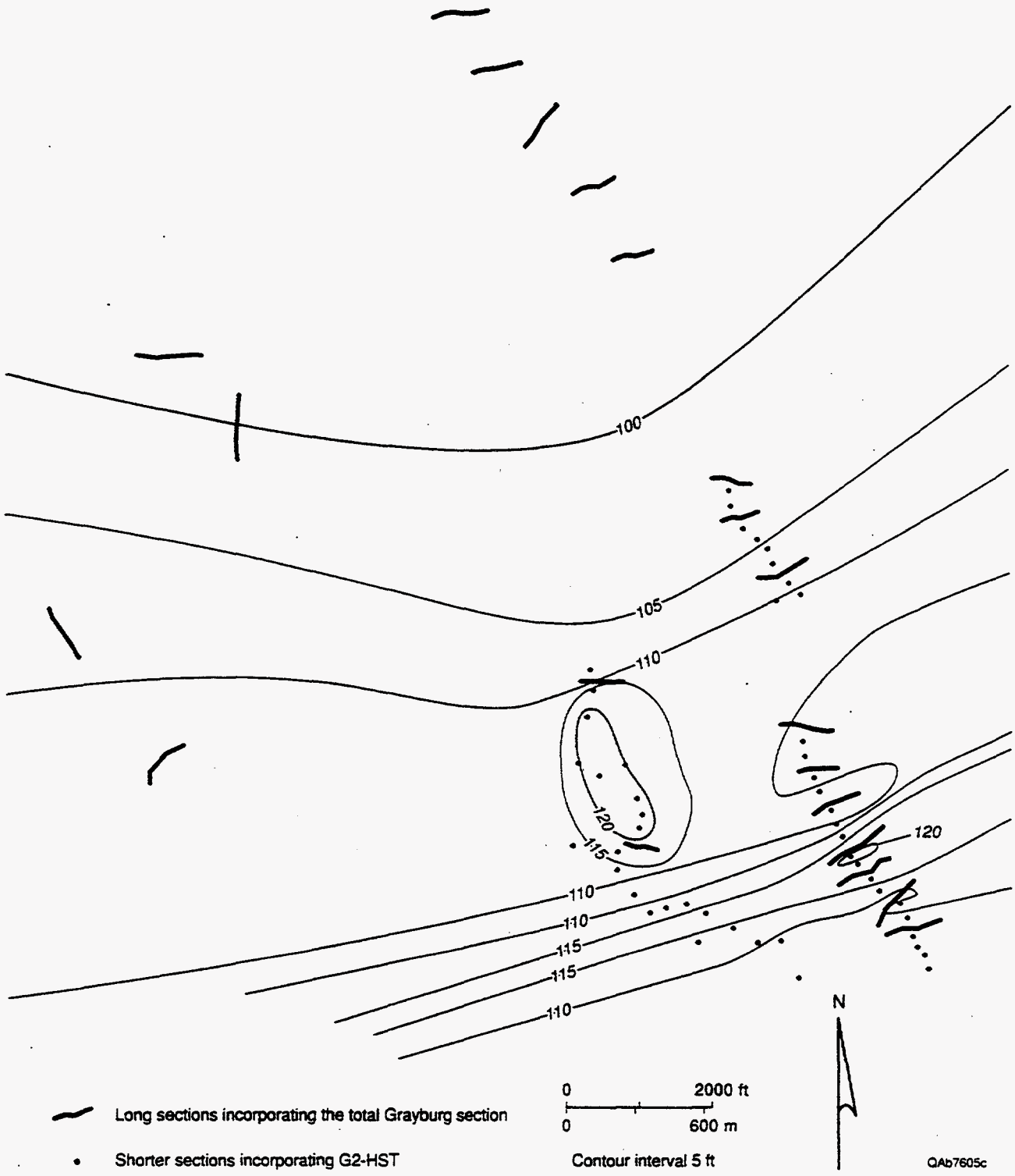

Figure 20. Isopach map of HFS 2 displays less pronounced basinward thickening of strata, recording infilling of much of the differential accommodation during deposition of HFS 1. Local isopach thick in West Dog Canyon represents depositional relief on a thick ramp crest that developed in this locale.

aggradational and consist of relatively restricted inner-to-middle ramp facies, and outer-ramp fusulinid-rich facies are not present. In more outer platform locations, however, such as Shattuck Valley (Kerans and Nance, 1991) and South Cowden field (Ruppel and Bebout, 1995), however, outer ramp fusulinid-peloid mud-dominated packstones and wackestones persist throughout HFS 3 (for example, see Fig. 15).

We designated the top of HFS 3 at the top of a laterally discontinuous tepee-fenestral-pisolitic unit that represents aggradation to a supratidal setting. This tidal flat unit is abruptly overlain by a skeletal-peloid mud-dominated packstone unit assigned to the base of HFS 4. However, because of the limited outcrop exposures of this interval in the study area (Fig. 7), this sequence boundary is poorly constrained.

Grayburg HFS 4 - The base of HFS 4 is a skeletal-peloid mud-dominated packstone. In the study area, there is poor outcrop control for much of HFS 4 (Fig. 7). The limited exposures are dominated by a limited suite of relatively restricted facies, including massive dolomitic quartz sandstone, peloidal wackestone and mud-dominated packstone, and tidal flats, suggesting that this interval consists of dominantly aggradational cycles that reflect limited accommodation during the late highstand of the Grayburg composite sequence. In Grayburg strata that accumulated seaward of the San Andres platform, however, outer ramp fusulinid-peloid packstone facies persist to the Grayburg-Queen sequence boundary (Kerans and Nance, 1991) because of greater accommodation in this periplatform succession. The Grayburg-Queen sequence boundary exhibits local paleokarst features and this unconformity is interpreted to represent a regional sequence boundary (Sarg and Lehmann, 1986). On Plowman Ridge, this surface is overlain by recessively weathered, yellow-brown to pink, thin-bedded sandstones assigned to the lowermost Queen Formation.

ARCHITECTURE OF A HIGH-FREQUENCY SEQUENCE: GRAYBURG HFS 2

Grayburg HFS 2 (Figs. 13 and 14) was selected for detailed stratigraphic analysis to delineate interwell-scale facies heterogeneity in the context of a high-resolution cycle-stratigraphic

framework. This high-frequency sequence is especially well exposed on Plowman Ridge and in West Dog Canyon, allowing construction of a three-dimensional image of facies heterogeneity along dip and across strike. Lastly, HFS 2 contains the greatest facies variability in the Grayburg composite sequence and exemplifies facies architecture within a high-frequency sequence.

The high-resolution chronostratigraphic framework established for Grayburg HFS 2 allowed confident correlation of each cycle between Plowman Ridge and West Dog Canyon. The overall stratigraphic succession is similar for the two locations, although they display differences in facies composition and cycle development (Figs. 13 and 14). These disparities reflect the slightly different platform location of the two cross-sections. The West Dog Canyon section is slightly updip of the Plowman Ridge section. This slight strike offset was imposed by the locations of suitable outcrop exposures of Grayburg HFS 2 on Plowman Ridge and in West Dog Canyon. Depositional variability across strike also accounts for differences between the two locations.

Grayburg HFS 2 contains 14 cycles arranged into 4 composite cycles (Figs. 13 and 14). The base of HFS 2 is an unconformable surface that developed on quartz sand-rich tidal flat facies at the top of HFS 1. This surface is considered to be a sequence boundary, because: (1) small-scale karst and erosional truncation along this surface record subaerial exposure during a substantial fall in relative sea level, and (2) outer ramp fusulinid-bearing facies at the base of HFS 2 indicate transgression and an abrupt landward facies tract offset. Grayburg HFS 2 is capped by tidal flat facies that record aggradation to supratidal conditions and infilling of accommodation. The top of this tidal flat unit is an unconformable surface that constitutes the upper sequence boundary. This surface is transgressed by outer ramp fusulinid-peloid mud-dominated packstones at the base of Grayburg HFS 3, recording an abrupt landward facies tract offset and maximum flooding in the Grayburg composite sequence.

Transgressive Systems Tract

Composite Cycle 2A - Composite cycle 2A (cycles 1, 2a, and 2b) records a transgressive-regressive succession during initial TST deposition (Figs. 13 and 14). Downdip fusulinid-bearing

peloid mud-dominated packstones at the base of cycle 1 (Fig. 13) record an abrupt facies tract offset above the HFS 1 sequence boundary. Cycle 1 locally shoals upward into quartzose peloid-ooid grainstones.

On Plowman Ridge, two cycles (cycles 2a and 2b), are recognized in the upper portion of composite cycle 2A (Fig. 13), whereas only one cycle (cycle 2) is recognized in West Dog Canyon (Fig. 14). Cycle 2a has a quartz sandstone base and is capped by ooid grainstone; cycle 2b is dominated by peloid-ooid mud-dominated packstone. In West Dog Canyon, this interval contains highly heterogeneous facies (Fig. 14), including laterally discontinuous channels, bars, and shoals composed of variable admixtures of quartz sandstone and ooid grainstone. Amalgamation of multiple cycles probably obliterated much of the cycle record in this interval due reworking in this high-energy tidal-dominated setting.

In West Dog Canyon near the top of composite cycle 2A, tidal flat facies are downcut 15 ft by a large channel with an abrupt erosional base (Fig. 14). This channel contains coarse ooid-intraclast grainstone and is oriented parallel to depositional dip (Fig. 16). The erosional incision is of uncertain origin, although its considerable (>15 ft) relief may imply that it represents a valley incised during a sea-level low. The carbonate sediment filling this channel contains no admixed quartz sand, in contrast with the adjacent quartz sand-dominated strata that the channel downcut, suggesting that the channel fill considerably postdates channel incision. This interpretation implies that at least two cycles occur within the upper portion of composite cycle 2A, one capped by the tidal flat facies and the second represented by the channel-fill sediments.

The top of composite cycle 2A is assigned to the top of the channel-fill deposits, which together with the adjacent, slightly older tidal flat facies, record maximum aggradation within this composite cycle. The upper bounding surface is abruptly overlain by a burrowed skeletal-peloid mud-dominated packstone to fusulinid-peloid mud-dominated packstone unit that records transgression at the base of composite cycle 2B (Figs. 13 and 14).

Composite Cycle 2B - Composite cycle 2B (cycles 3, 4, and 5) is a transgressive-regressive succession that records continued TST deposition. The base of cycle 3 is a fusulinid-peloid mud-

dominated packstone unit that represents a landward facies tract offset (Figs. 13 and 14). This fusulinid-peloid mud-dominated packstone unit grades updip in West Dog Canyon into a thin unit of burrowed skeletal-peloid mud-dominated packstones. Cycle 3 is locally capped by an accretionary ooid grainstone bar, recording aggradation into a high-energy subtidal setting. This grainstone bar passes downdip into equivalent low-energy burrowed peloid-ooid grain-dominated packstone and fusulinid-peloid mud-dominated packstone facies.

The upper two cycles in composite cycle 2B, cycles 4 and 5, contain abundant massive and cross-stratified quartz sandstone (Figs. 13 and 14), recording eolian quartz sand deposition during cyclic sea level lowstands and subsequent subtidal reworking. Cycles 4 and 5 pass upward into local ooid grainstone shoals. The top of composite cycle 2B is a laterally discontinuous tidal flat dolomite to quartz sandstone unit, with locally abundant fenestrae, pisoids, and desiccation cracks. This facies represents aggradation to sea level; the upper bounding surface of cycle 5 is designated to be the top of composite cycle 2B and is abruptly overlain by transgressive skeletal-peloid mud-dominated packstone at the base of composite cycle 2C.

Maximum Flooding and Initial Highstand Systems Tract

Composite Cycle 2C - Composite cycle 2C (cycles 6, 7, 8, 9, 10) records a transgressive-regressive succession during maximum accommodation and early HST deposition. Burrowed skeletal-peloid mud-dominated packstone in the lowermost cycles 6 and 7 record successive flooding of the platform (Figs. 13 and 14). Cycle 8 is a widespread fusulinid-peloid mud-dominated packstone that represents maximum flooding in HFS 2. Cycles 6 through 8 are dominated by carbonate due to widespread flooding that limited eolian siliciclastic influx.

Cycles 9 and 10 record the onset of highstand deposition and cyclic aggradation to high-energy subtidal conditions. These two cycles contain a basal burrowed skeletal-peloid mud-dominated packstone to dolomitic massive quartz sandstone with locally abundant fusulinids. These low-energy subtidal facies shoal upward into peloid-ooid grain-dominated packstone capped by ooid grainstone (Figs. 13 and 14). The top of composite cycle 2C is placed at the top of

cycle 10 because in downdip locations along Plowman Ridge (Fig. 13) this surface is abruptly transgressed by a quartzose fusulinid-peloid mud-dominated packstone unit that grades updip into a fusulinid-bearing dolomitic massive sandstone and because a thick sandstone succession, recording a fall in sea level, immediately overlies cycle 10.

Late Highstand Systems Tract

Composite Cycle 2D - Composite cycle 2D (cycles 11, 12, and 13) records a transgressive-regressive succession that developed during late HST deposition. In the downdip portion of Plowman Ridge (Fig. 13), cycle 11 contains a transgressive base of fusulinid-peloid mud-dominated packstone that grades landward into fusulinid-bearing dolomitic massive sandstones. The top of cycle 11 is capped by an updip ooid grainstone unit in West Dog Canyon (Fig. 14) that grades immediately downdip into a massive quartz sandstone succession in which this cycle cap is poorly defined and is represented by a stratal surface with local borings and *Thalassinoides*-type burrows. On Plowman Ridge, the top of cycle 11 is a quartzose peloid packstone (Fig. 13).

The upper portion of composite cycle 2D consists of aggradational and progradational cycles dominated by ooid grainstone (Figs. 13 and 14). Cycle 12 contains basal dolomitic massive quartz sandstone to quartzose peloidal mud-dominated packstone facies that shoal upward into peloid-ooid grain-dominated packstone and capping ooid grainstone. These ooid grainstones represent the best developed grainstone bodies in the Grayburg. For example, the ooid grainstone body in cycle 12 attains a maximum thickness of 14 ft and forms a strike-elongate shoal (Fig. 17). The shoal has a dip width of more than 4,000 ft and extends for at least 3,000 ft across strike. Landward, this grainstone thins and grades into peloid-ooid mud-dominated packstones and dolomitic sandstones. Platform aggradation to supratidal environments in cycle 13 is recorded by ramp crest tidal flat facies. The supratidal ramp crest was flanked seaward by high-energy ooid grainstones. The erosional surface capping HFS 2 is abruptly transgressed by outer ramp fusulinid mud-dominated packstone, recording maximum flooding in the Grayburg composite sequence.

RELATIONSHIP OF CYCLES AND FACIES WITH LONGER TERM ACCOMMODATION TRENDS

Cycle Thickness and Facies Volumes

Cycle thickness and facies stacking patterns in Grayburg HFS 2 reflect the complex interplay of accommodation space and sediment supply imposed by platform position and three orders of sea level fluctuations: cycles; composite cycles; and high-frequency sequences, superimposed on the longer term composite sequence. Figure 21 displays relative sediment volumes computed for each cycle using the two-dimensional dip sections from Plowman Ridge and West Dog Canyon. The trends defined by relative sediment volume and facies proportions are similar for the two locations, reinforcing the cycle-scale correlations. Differences in thickness and facies content, in part, reflect depositional variability across strike as well as the different platform location of the two cross sections. The West Dog Canyon section is slightly updip of the Plowman Ridge section, which extends for approximately another 2,000 ft downdip.

The cycle sediment volume (e.g., thickness) stacking patterns for Grayburg HFS 2 do not display a clear relationship with longer-term accommodation imposed by the high-frequency sequence (Fig. 21). This is chiefly because Grayburg cycles did not typically aggrade to sea level and fill accommodation as is assumed by one-dimensional models relating cycle stacking patterns to longer-term stratigraphic sequences. Such models dictate that the transgressive systems tract should contain successively thicker cycles, reflecting progressive increase in accommodation during flooding and the highstand systems tract should contain upward-thinning cycles as accommodation was increasingly filled, which is not the case for the Grayburg (Fig. 21).

Facies-specific sedimentation rates influenced the potential of individual cycles to aggrade to sea level. For example, siliciclastic-dominated cycles, because of their lower inherent sedimentation rate relative to carbonate cycles, were less likely to completely fill accommodation and aggrade to sea level. Moreover, lower sedimentation rates during periods of maximum flooding resulted in deposition of relatively thin (condensed) cycles despite the concomitant

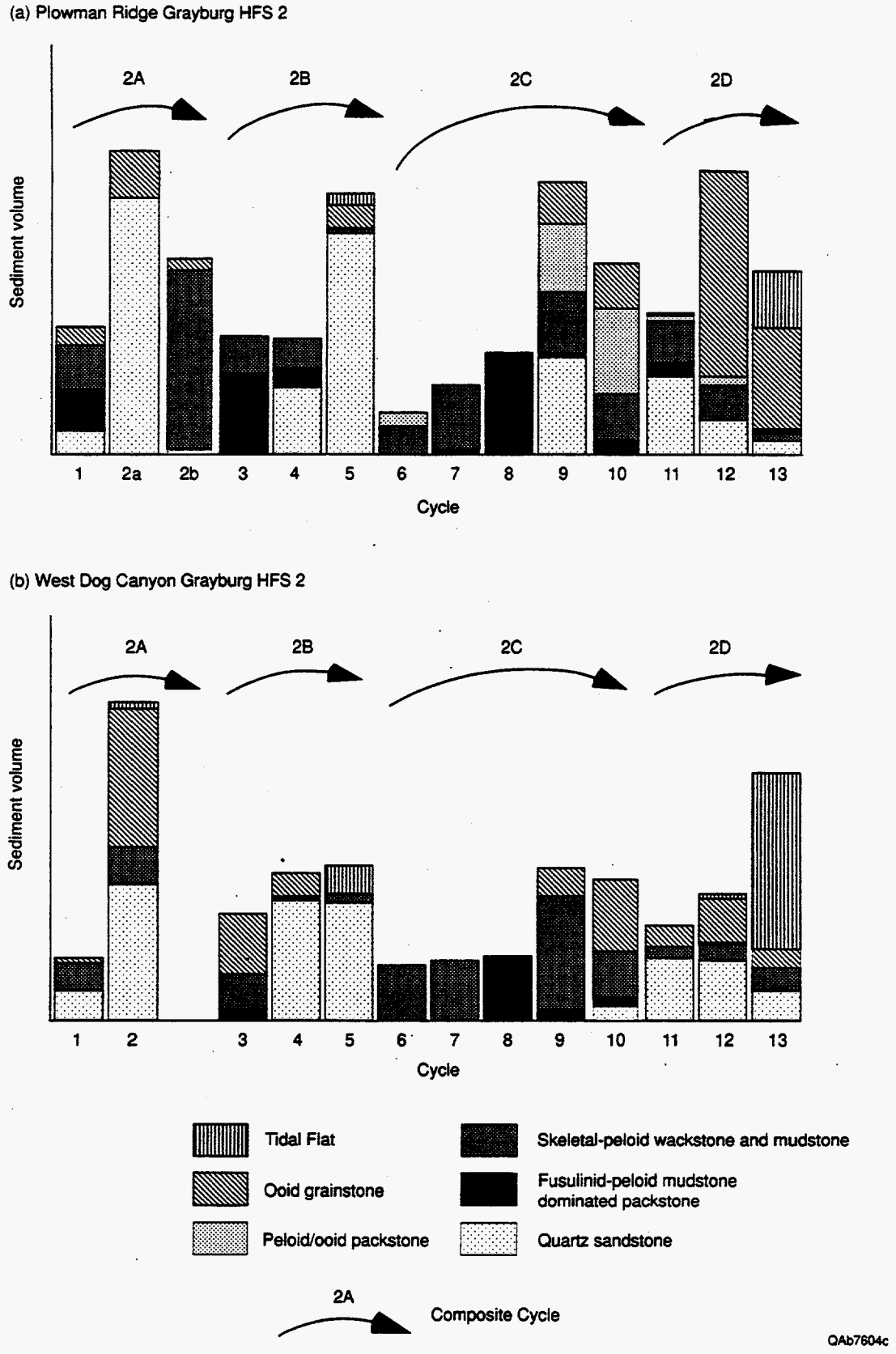

Figure 21. Sediment and facies proportions for Grayburg HFS 2 cycles computed from Plowman Ridge and West Dog Canyon cross sections. Grayburg cycles did not typically aggrade to sea level and fill accommodation. Cycle thickness stacking patterns, therefore, do not display a good relationship with long-term accommodation imposed by high-frequency sequences.

increase in accommodation induced by a rise in relative sea level. In Grayburg HFS 2, this is most strikingly displayed by cycle 8, a widespread fusulinid-peloid mud-dominated packstone condensed interval composed of up to 40 percent fusulinids.

Another factor complicating cycle stacking analysis is incomplete preservation of the cyclic record, such as unrecognized amalgamation of multiple cycles. Unusually thick cycles, especially in the high-energy tidal-dominated early transgressive systems tract (composite cycle 2A) and in the accommodation-limited late highstand systems tract (composite cycle 2D) likely record reworking and amalgamation of one or more cycles.

Figure 21 shows that cycle stacking trends within Grayburg HFS 2 define an intermediate-scale cyclicity of composite cycles. The transgressive cycle at the base of each composite cycle is thin and consists of predominantly low-energy subtidal facies. Successive cycles in the composite cycle are thicker and increasingly composed of shallow-water facies, recording increased sedimentation and progressive filling of accommodation. In some composite cycles, the uppermost cycles are thinner, probably as a result of decreasing accommodation.

OUTCROP-BASED POROSITY AND PERMEABILITY

To assess lateral porosity and permeability heterogeneity within potential reservoir flow units, dip-oriented core plug transects were sampled on Plowman Ridge and West Dog Canyon from analog reservoir flow units in Grayburg HFS 2. In cycle 10, an ooid grain-dominated packstone unit in the upper portion of the cycle was sampled (for example, Fig. 22). In cycle 12, an ooid grainstone unit was sampled (for example, Fig. 23). Both sampled units exhibit the lateral continuity typical of this highstand setting.

At Plowman Ridge samples were collected from the two facies in cycles 10 and 12 along horizontal traverses of 580 and 515 ft respectively, at 5 ft intervals (Figs. 24 and 25). Three vertical plug traverses at 1 ft spacing were also collected from each facies. At West Dog Canyon the same two cycles were sampled along horizontal traverses of 610 and 535 ft, also at 5 ft

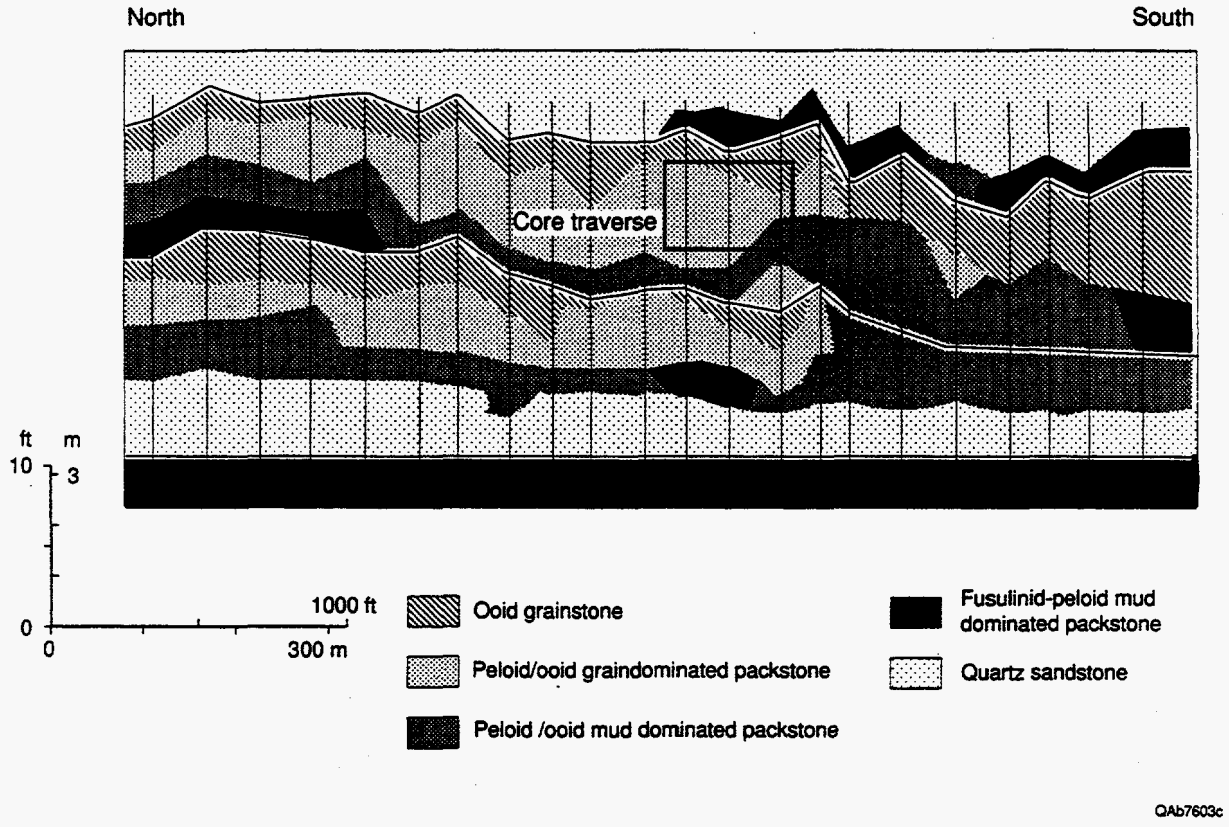

Figure 22. Stratigraphic cross section detailing cycles 9 and 10 in HFS 2 on Plowman Ridge. Cycles 9 and 10 represent early highstand deposition. The rectangle in cycle 10 indicates location of horizontal traverse sampled to assess lateral heterogeneity of porosity and permeability within this grain-dominated packstone unit.

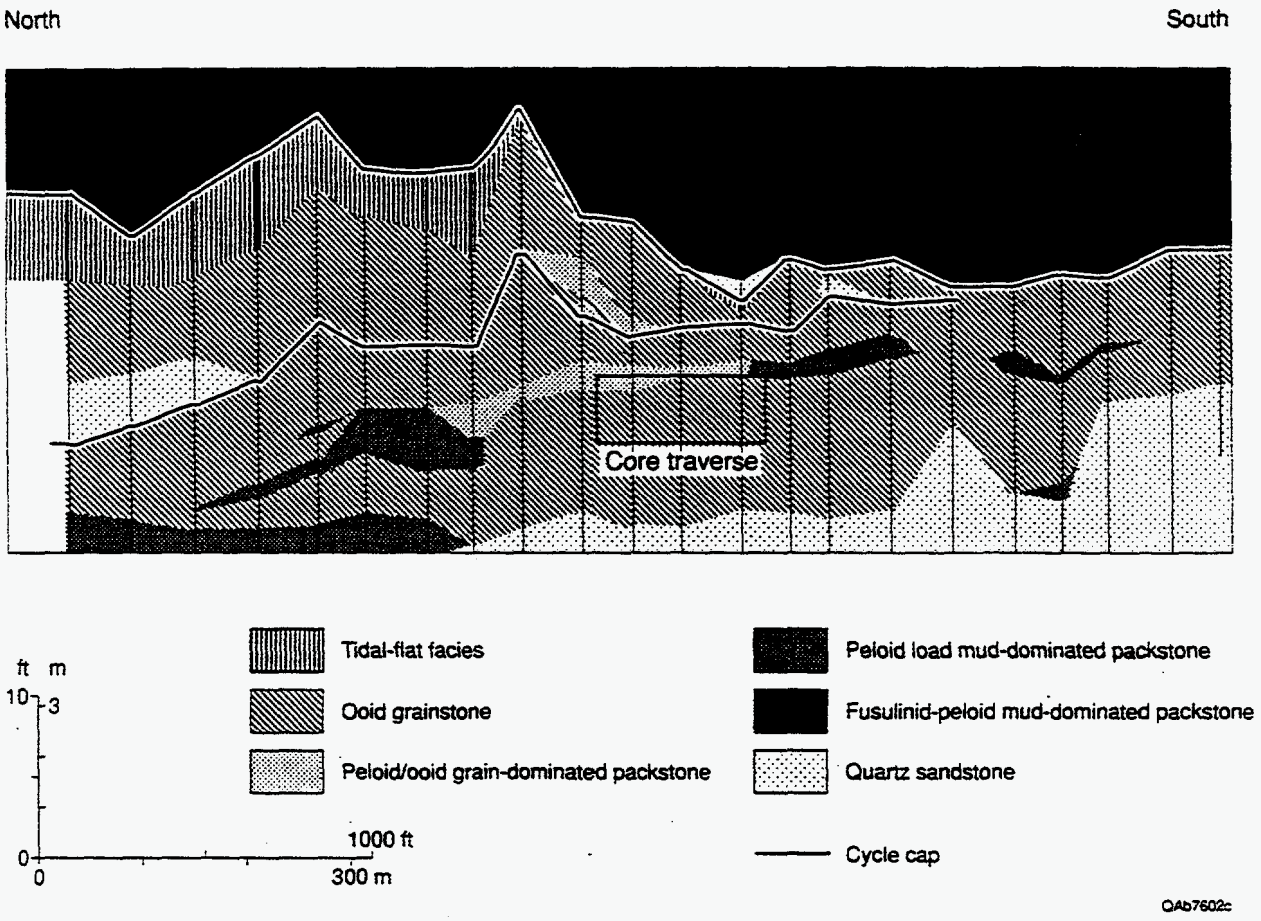

Figure 23. Stratigraphic cross section detailing cycles 12 and 13 in HFS 2 on Plowman Ridge. Cycles 12 and 13 represent late highstand deposition and are dominated by ooid grainstone. The rectangle in cycle 12 indicates location of horizontal traverse sampled to assess lateral heterogeneity of porosity and permeability within this grainstone unit.

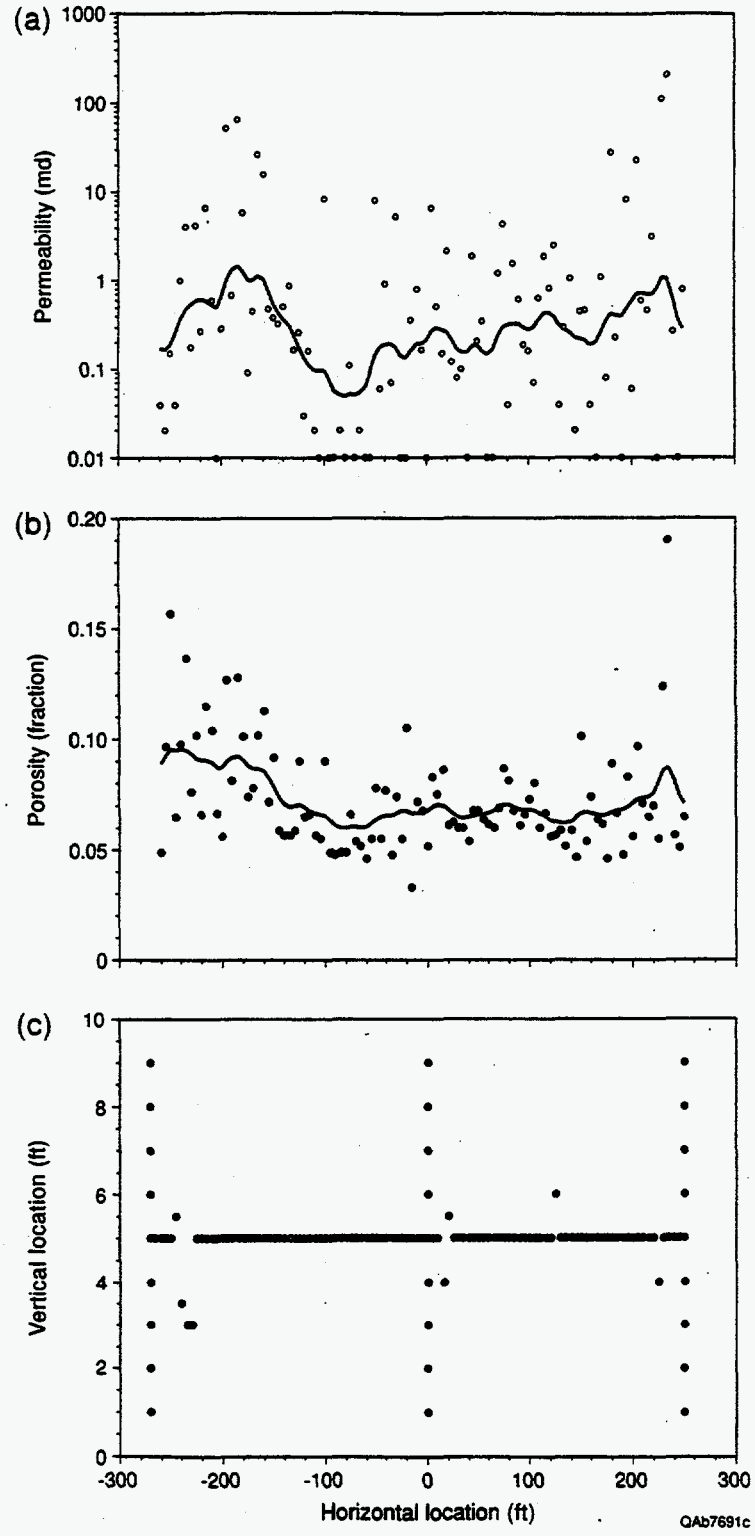

Figure 24. Permeability, porosity, and sample locations for samples collected from cycle 10 at Plowman Ridge. The permeability and porosity graphs show plug measurements (points) and a smoothed trace (curve) to aid visualization of the larger scale trends. The sampling included three vertical transects that were not used in horizontal variography and do not appear in these displays.

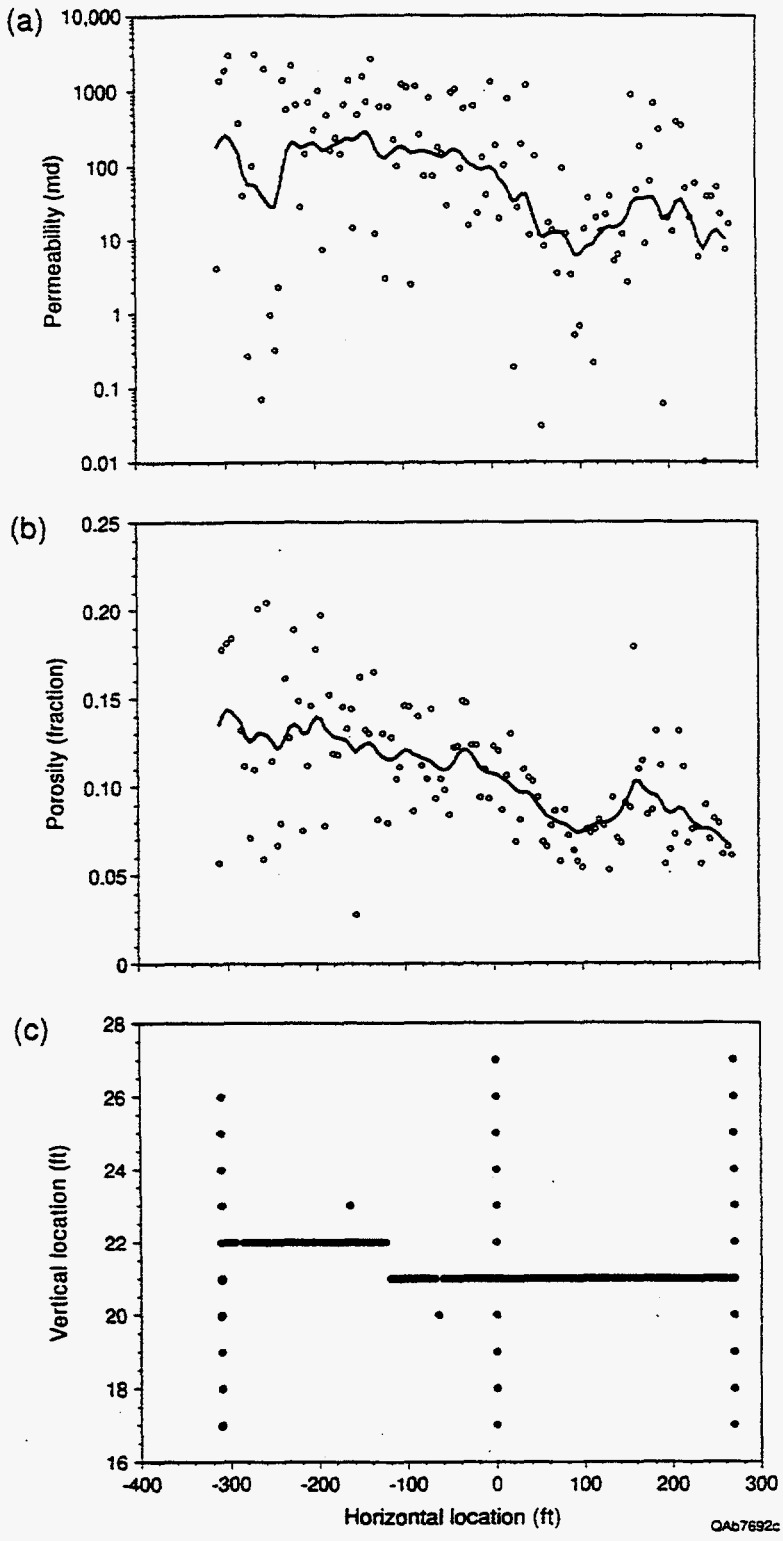

Figure 25. Permeability, porosity, and sample locations for samples collected from cycle 12 at Plowman Ridge. The permeability and porosity graphs show plug measurements (points) and a smoothed trace (curve) to aid visualization of the larger scale trends. The sampling included three vertical transects that were not used in horizontal variography and do not appear in these displays.

intervals (Figs. 26 and 27), but closely spaced vertical transects were not sampled there as at Plowman Ridge. The samples at West Dog Canyon were cut into several one-inch pieces where possible to evaluate any observable differences in surface weathering effects within the first several inches of the outcrop surface and to provide a measurement of variability at the one-inch scale. Both porosity and permeability exhibit a high degree of variability in each transect. The cycle 12 transect at West Dog Canyon crosses a small fault between 270 and 315 feet where both porosity and permeability are unusually high (Fig. 27). These data are believed to be influenced by fault and fracture-associated dissolution effects and were excluded from further analysis.

As expected, the grain-dominated packstones at Plowman Ridge are generally less permeable than the grainstones (Fig. 28a) because of the presence of interparticle carbonate mud. The grainstones contain abundant interparticle primary porosity, much of which is preserved. Thus, the geometric average permeability in cycle 12 is about two orders of magnitude larger than in cycle 10, and the two units have distinct, although overlapping data clouds on a porosity-permeability cross plot (Fig. 28a). However, the same relationship is not observed at West Dog Canyon. The same two units at this location have nearly the same porosity and permeability histograms (Fig. 28b). Further examination of thin sections from West Dog Canyon is expected to verify that the cycle 10 grain-dominated packstone exposure there is adversely affected by dissolution. However, multiple samples at West Dog Canyon do not show any statistically significant differences within the first few inches of the outcrop surface, so the dissolution effects are probably not associated with near surface weathering except perhaps in the vicinity of faults and fractures.

Variograms computed for each horizontal transect display a variety of structures for separations greater than about 150 ft. However, these "long-range" structures represent a significant fraction of the total length of each transect, and thus they may merely represent a different statistical accident at each location. Nevertheless, the "short-range" variograms (less than 150 ft) are similar. This similarity is emphasized in figures 29 and 30 by combining the data from all four transects into a single variogram after a separate Gaussian transformation at each location.

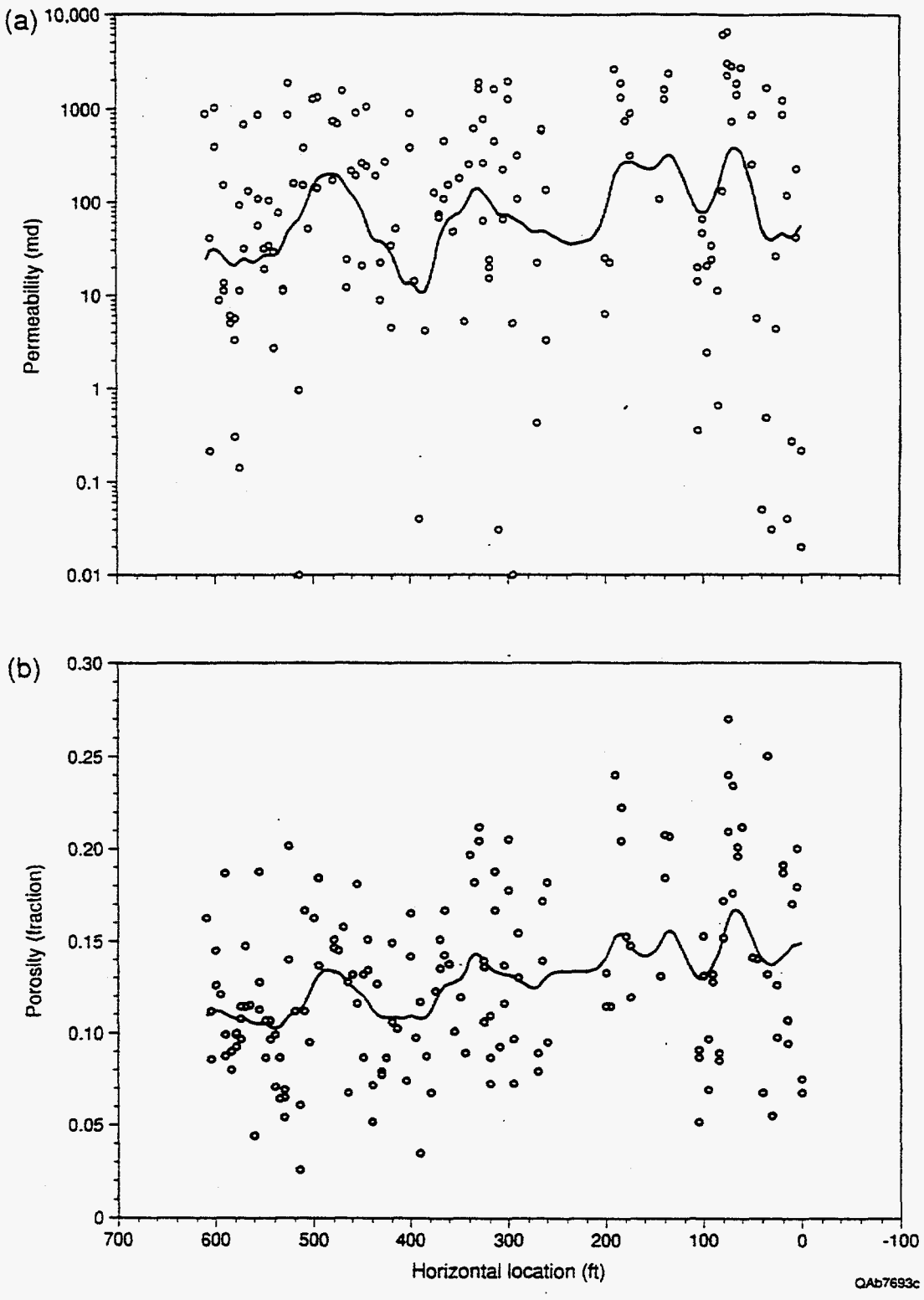

Figure 26. Permeability and porosity for samples collected from cycle 10 at West Dog Canyon. The permeability and porosity graphs show plug measurements (points) and a smoothed trace (curve) to aid visualization of the larger scale trends.

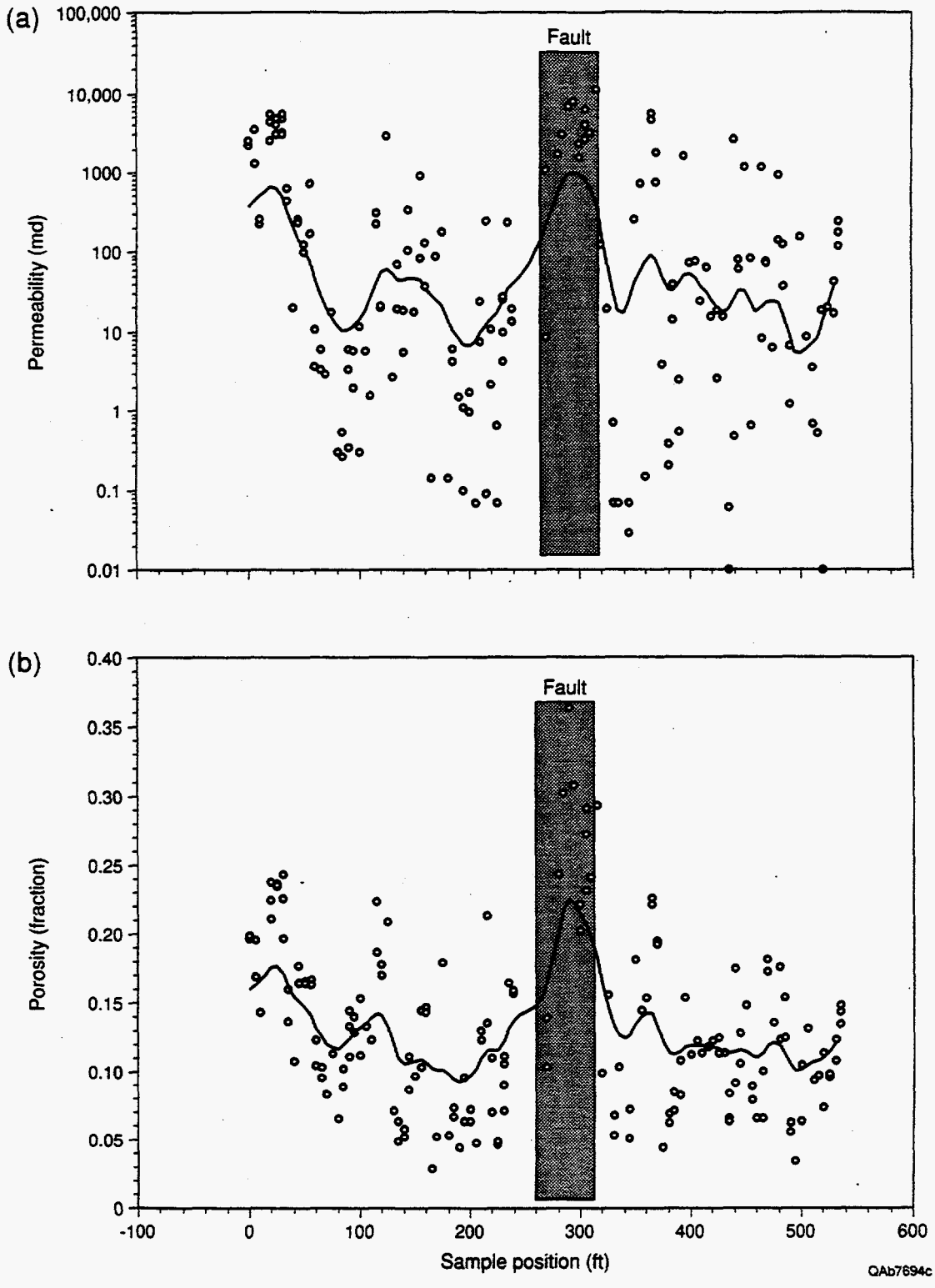

Figure 27. Permeability and porosity for samples collected from cycle 12 at West Dog Canyon. The permeability and porosity graphs show plug measurements (points) and a smoothed trace (curve) to aid visualization of the larger scale trends. Sample locations between 270 and 315 feet were eliminated from further analysis because of dissolution effects associated with a small fault crossing the transect.

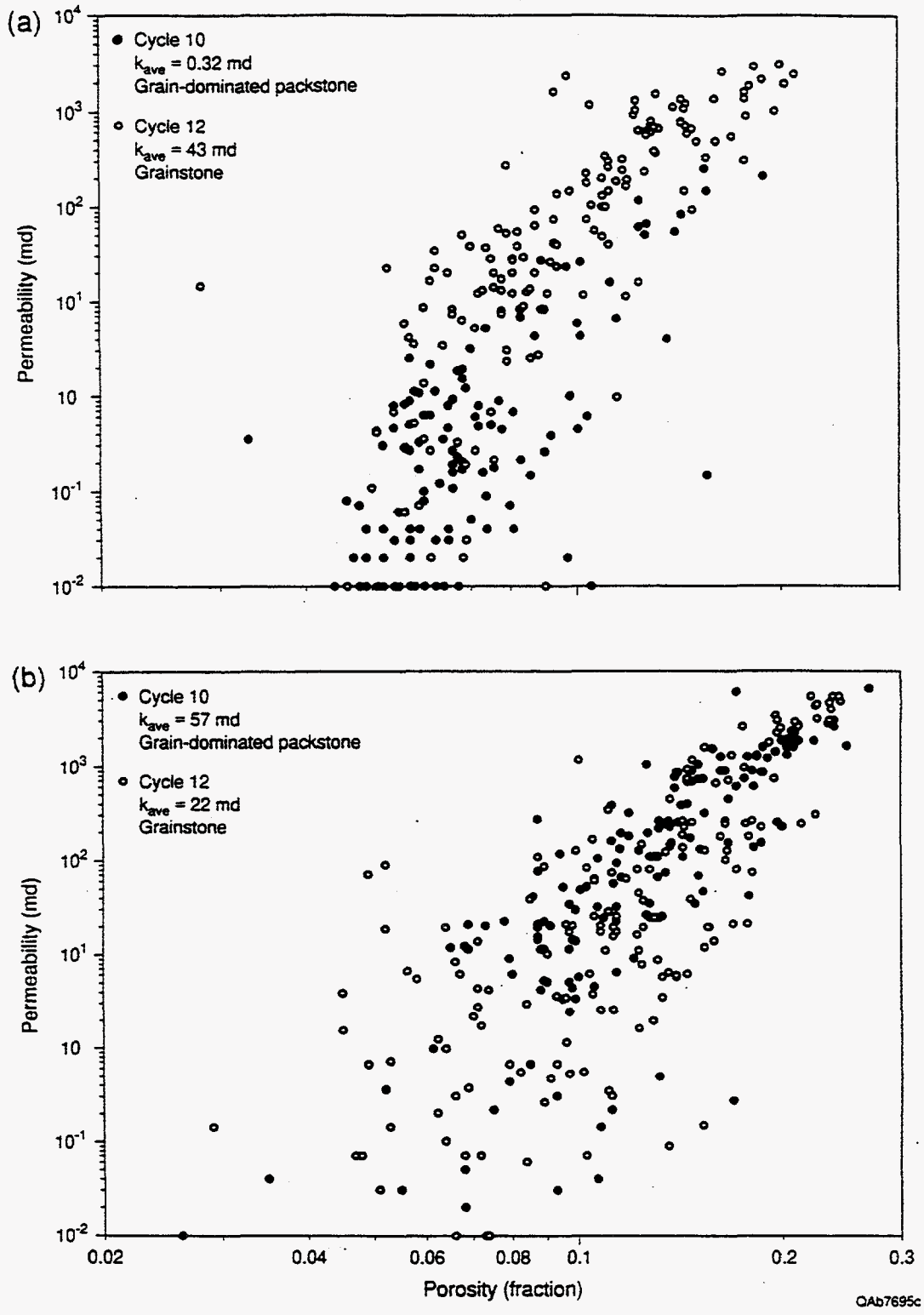

Figure 28. Porosity and permeability cross plots for Plowman Ridge (a) and West Dog Canyon (b).

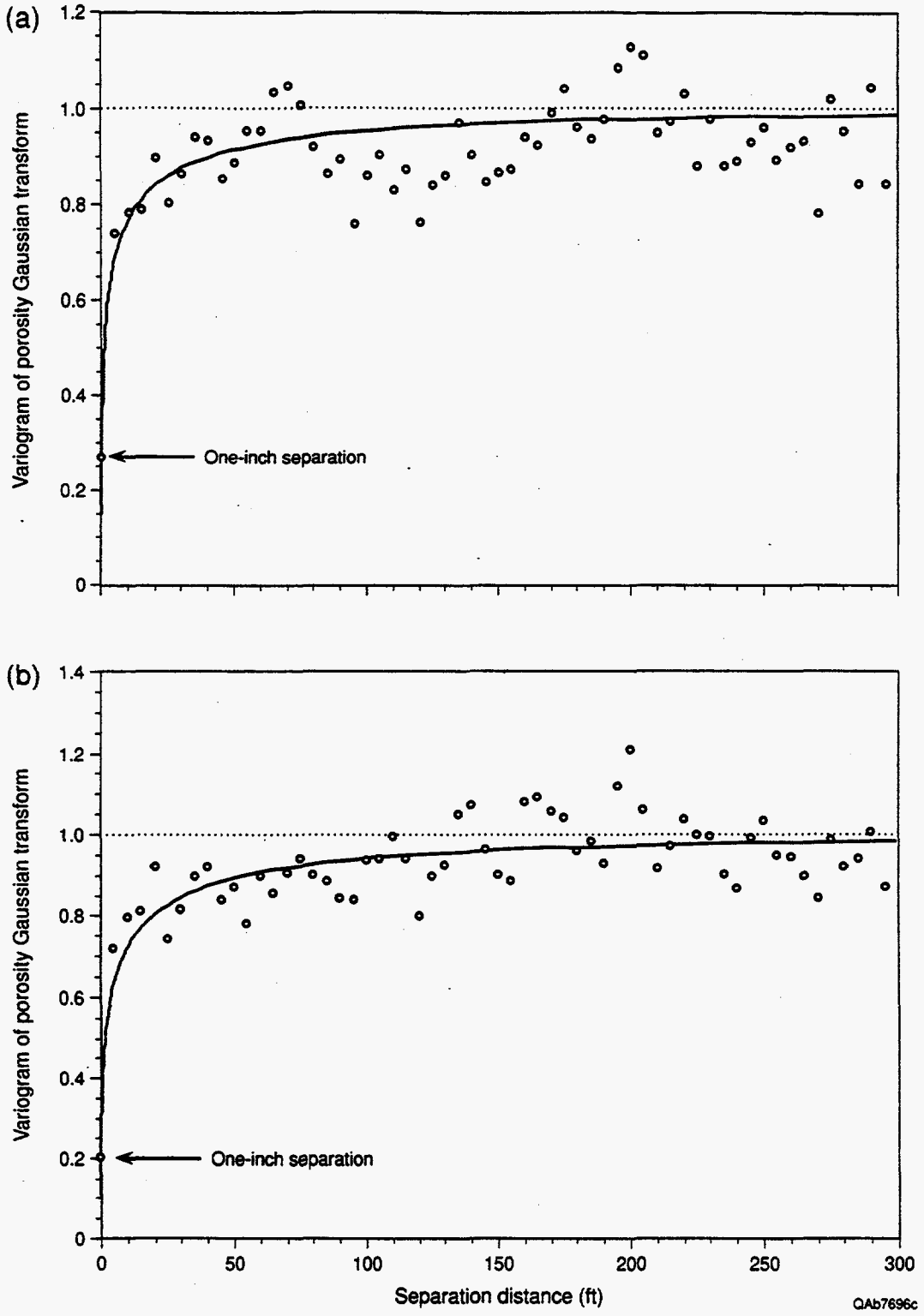

Figure 29. Semivariograms, on a Cartesian scale, of the Gaussian transforms of permeability and porosity for all four horizontal transects at Plowman Ridge and West Dog Canyon. The measurements are shown as points, a model described in the text as a solid curve, and the overall variance (sill) as a dashed line.

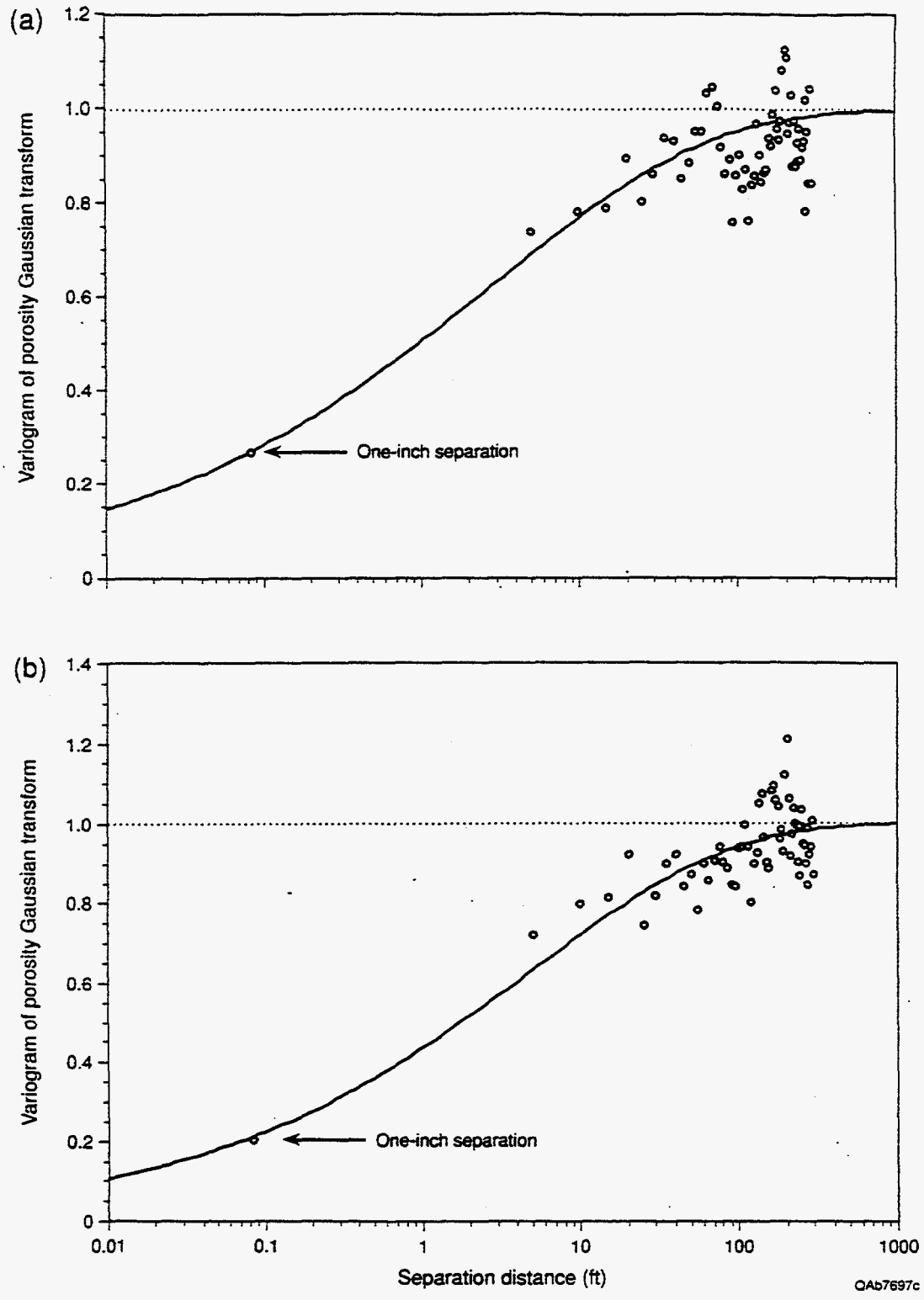

Figure 30. Semivariograms, on a logarithmic scale, of the Gaussian transforms of permeability and porosity for all four horizontal transects at Plowman Ridge and West Dog Canyon. The measurements are shown as points, a model described in the text as a solid curve, and the overall variance (sill) as a dashed line.

This device improves the statistical significance of the measurement by increasing the number of data pairs, and the different long-range structures are effectively canceled out, giving a single average variogram. The Gaussian transforms remove effects of different averages and variances at each location, focusing attention on the correlation structure itself. In any case, the Gaussian transform is a required step if the variogram is to be used in Gaussian simulation.

The variograms exhibit a concentration of variance at relatively small scales, an observation common in carbonate outcrops (Senger and others, 1991; Grant and others, 1994; Wang and others, 1994). As a first approximation, the variograms could be modeled as a pure nugget. However, the sample pairs with one-inch spacing at West Dog Canyon display a significantly smaller variance than the five-foot and larger spacings, indicating a significant correlation structure with a range between one inch and five feet.

Both the porosity and permeability variograms can be approximated with very similar models:

$$\gamma_{\phi}(\mathbf{h}) = 1 - \exp\left[-(h/5)^{0.35}\right]$$

and

$$\gamma_{k}(\mathbf{h}) = 1 - \exp\left[-(h/3)^{0.32}\right]$$

where γ_{ϕ} and γ_{k} are the dimensionless variograms of the Gaussian transforms of porosity and permeability, and h is the horizontal separation distance in feet. In Figure 30 the variograms and models are displayed on logarithmic coordinates for better visualization of the short-range behavior. Additional sampling would be required to verify the anticipated structure between one-inch and five-foot separations.

SUMMARY

This outcrop study of the Grayburg Formation documents three levels of stratigraphic hierarchy (high-frequency sequences, composite cycles, and cycles) within the Grayburg composite sequence. This stratigraphic hierarchy is defined by: (1) transgressive-regressive

relationships expressed along a dip-oriented cross-section; (2) vertical and lateral facies stacking patterns; (3) abrupt facies tract offsets; and (4) lateral tracing of unconformable stratal surfaces. Crucial facies for interpreting the longer term accommodation trends include: (1) outer ramp fusulinid-peloid mud-dominated packstone and wackestone facies that record maximum transgression; (2) ramp crest ooid grainstones that represent aggradation to high-energy subtidal environments and thus provide a record of accommodation trends through time; (3) tidal flat facies that indicate platform aggradation to sea level; and (4) eolian-transported quartz sands that reflect widespread emergence of the shallow platform during sea-level lowstands.

The four high-frequency sequences documented within the Grayburg composite sequence by this outcrop study display similar stratigraphic architecture and facies development to that of the subsurface productive Grayburg on the Central Basin Platform, providing a basis for correlation between the subsurface and the outcrop analogs. The detailed three-dimensional image of stratigraphic architecture and geological heterogeneity developed by this outcrop study are thus directly applicable to productive Grayburg reservoirs.

Grayburg high-frequency sequences are composed of several composite cycles that are transgressive-regressive successions that contain multiple cycles. Composite cycles form chronostratigraphic units that generally can be readily recognized and correlated using subsurface log and core data. Cycles are vertical upward-shoaling facies successions that form the basic chronostratigraphic unit for high-resolution correlation and delineation of geological heterogeneity. Cycles, however, can be difficult to identify and confidently correlate throughout a field using typical subsurface data, whereas the greater facies tract offsets recorded by the composite cycles allow more confident chronostratigraphic subdivision of the high-frequency sequences. This composite cycle correlation framework can also form the basis of further subdivision into constituent cycles.

The stratigraphic setting strongly influenced facies distribution and lateral heterogeneity. For example, permeable ooid grainstones that accumulated in a transgressive setting formed dip-elongate tidal channels and bars. Conversely, ooid grainstones that accumulated under highstand

conditions formed strike-elongate shoals that are laterally continuous along dip and across strike for thousands of feet. The well-defined relationship between stratigraphic hierarchy and facies composition and heterogeneity can be used to improve subsurface correlations and better predict lateral dimensions of reservoir facies.

Lateral heterogeneity of porosity and permeability at the interwell-scale was evaluated by core plug sampling along dip-oriented traverses from ooid grain-dominated packstone and grainstone units. The semivariograms for porosity and permeability display a large component of uncorrelated variability across distances less than 150 ft with a significant correlation structure at a range between 1 inch and 5 ft. The variograms also display a smaller component of variability with long range correlations beyond the several hundred feet transect. It is possible that this large-scale correlation structure can be identified using well data.

ACKNOWLEDGMENTS

C. Kerans and F. J. Lucia proposed this study, obtained research support, and contributed greatly to the concepts and interpretations throughout the course of the project. We thank S. C. Ruppel and W. M. Fitchen for contributing their insight and ideas. Jubal G. Grubb, Milton H. Kwong, Kirt A. Kempter, and Radu Boghici served as research and field assistants. Funding for this research was provided by the U.S. Department of Energy and by the Industrial Associates of the Reservoir Characterization Research Laboratory.

REFERENCES

Babcock, J. A., 1977, Calcareous algae, organic boundstones, and the genesis of Upper Capitan Limestone (Permian, Guadalupian), Guadalupe Mountains, West Texas and New Mexico, *in* Hileman, M. E., and Mazzullo, S. J., eds., Upper Guadalupian Facies, Permian Reef

Complex, Guadalupe Mountains, New Mexico and West Texas: Permian Basin Section, SEPM Publication 77-16, p. 3-44.

Barnaby, R. J., and Ward, W. B., 1995, Sequence stratigraphic framework, high-frequency cyclicity and three-dimensional heterogeneity: Grayburg Formation, Brokeoff Mountains, New Mexico: *in* Pause, P. H., and Candelaria, M. P., (eds.), Carbonate Facies and Sequence Stratigraphy: Practical Applications of Carbonate Models: PBS–SEPM Publication 95-36, p. 37-50.

Boyd, D. W., 1958, Permian Sedimentary Facies, Central Guadalupe Mountains, New Mexico: New Mexico Bureau of Mines and Mineral Resources Bull. 49, 100 p.

Dickey, R. I., 1940, Geologic section from Fisher County through Andrews County, Texas, to Eddy County, New Mexico: AAPG Bull. 24, p. 1-14.

Dunham, R. J., 1962, Classification of carbonate rocks according to depositional texture, *in* Ham, W. E., ed., Classifications of carbonate rocks—a symposium: AAPG Memoir 1, p. 108-121.

Fekete, T. E., Franseen, E. K., Pray, L. C., 1986, Deposition and erosion of the Grayburg Formation (Guadalupian, Permian) at the shelf-to-basin margin, western escarpment, Guadalupe Mountains, Texas, *in* Moore, G. E., and Wilde, G. L., eds., Lower and Middle Guadalupian Facies, Stratigraphy, and Reservoir Geometries, San Andres-Grayburg Formations, Guadalupe Mountains, New Mexico and Texas: Permian Basin Section, SEPM Special Publication 86-25, p. 69-81.

Fischer, A. G., and Sarnthein, M., 1988, Airborne silts and dune-derived sands in the Permian of the Delaware Basin: Journal of Sedimentary Petrology, v. 58, p. 637-643.

Fitchen, W. M., 1992, Sequence stratigraphy of the upper San Andres Formation and Cherry Canyon Tongue (Permian, Guadalupian), southern Brokeoff Mountains, New Mexico: unpublished M.A. thesis, The University of Texas at Austin, 155 p.

Fitchen, W. M., 1993, Sequence stratigraphic framework of the Upper San Andres Formation and equivalent basinal strata in the Brokeoff Mountains, Otero County, New Mexico: New Mexico

Geological Society Guidebook, 44th Field Conference, Carlsbad Region, New Mexico and West Texas, p. 185-193.

Franseen, E. K., Fekete, T. E., and Pray, L. C., 1989, Evolution and destruction of a carbonate bank at the shelf margin: Grayburg Formation (Permian), western escarpment, Guadalupe Mountains, Texas, *in* Crevello, P. D., Wilson, J. L., Sarg, J. F., and Read, J. F., eds., Controls on Carbonate Platform and Basin Development: SEPM Special Publication No. 44, p. 289-304.

Galloway, W. E., Ewing, T. E., Garrett, C. M., Tyler, Noel, and Bebout, D. G., 1983, Atlas of major Texas oil reservoirs: The University of Texas at Austin, Bureau of Economic Geology, 139 p.

Grant, C. W., Goggin, D. J., and Harris, P. M., 1994, Outcrop analog for cyclic-shelf reservoirs, San Andres Formation of Permian Basin: stratigraphic framework, permeability distribution, geostatistics, and fluid-flow modeling: AAPG Bull., v. 78, p. 23-54.

Harris, P. M., Kerans, C., and Bebout, D. G., 1993, Ancient outcrop and modern examples of platform carbonate cycles–implications for subsurface correlation and understanding reservoir heterogeneity: *in*, Loucks, R. G., and Sarg, J. F., (eds.), Carbonate Sequence Stratigraphy, AAPG Memoir 57, p. 475-492.

Hayes, P. T., 1959, San Andres Limestone and related Permian rocks in Last Chance Canyon and vicinity, southeastern New Mexico: AAPG Bull., v. 43, p. 2197-2213.

Hayes, P. T., 1964, Geology of the Guadalupe Mountains, New Mexico: U.S. Geol. Survey Prof. Paper 446, 69 p.

Hovorka, S. D., Nance, H. S., and Kerans, C., 1993, Parasequence geometry as a control on porosity evolution: examples from the San Andres and Grayburg Formations in the Guadalupe mountains: *in* Loucks, R. G., and Sarg, J. F., eds., Carbonate Sequence Stratigraphy: Recent Development and Applications: AAPG Memoir 57, p. 493-514.

Kerans, C., 1992, Chapter II: Outcrop Delineation of Carbonate Sand Body Distribution in a Sequence-Stratigraphic Framework, *in* Tyler, N., Barton, M. D., Bebout, D. G., Fisher,

R. S., Grigsby, J. D., Guevara, E., Holtz, M., Kerans, C., Nance, H. S., and Levey, R. A.: Characterization of Oil and Gas Reservoir Heterogeneity, Final DOE Report, Contract No. DE-FG22-89BC14403, p. 7-39.

Kerans, C., and Fitchen, W. M., 1995, Sequence hierarchy and facies architecture of a carbonate-ramp system: San Andres Formation of Algerita Escarpment and Western Guadalupe Mountains, West Texas and New Mexico: Bureau of Economic Geology Report of Investigations No. 235, The University of Texas at Austin, 86 p.

Kerans, C., Fitchen, W. H., Gardner, M. S., Sonnenfeld, M. D., Tinker, S. W., and Wardlaw, B. R., 1992a, Styles of sequence development within uppermost Leonardian through Guadalupian strata of the Guadalupe Mountains, Texas and New Mexico, *in* Mruk, D. H., and Curran, B. C., eds., Permian Basin Exploration and Production Strategies: Applications of Sequence Stratigraphic and Reservoir Characterization Concepts, West Texas Geological Society Symposium, Publication 92-91, p. 1-7.

Kerans, C., Fitchen, W. M., Gardner, M.S., and Wardlaw, B. R., 1993, A contribution of evolving stratigraphic framework of Middle Permian strata of the Delaware basin, Texas and New Mexico, *in* Love, D. W., and others, eds., New Mexico Geological Society Guidebook, 44th field Conference, Carlsbad Region, New Mexico and Texas, p: 175-184.

Kerans, C., Lucia, F. J., and Senger, R. K., 1994, Integrated characterization of carbonate ramp reservoirs using Permian San Andres Formation outcrop analogs: AAPG Bull. 78, p 181-216.

Kerans, C., and Nance, H. S., 1991, High-frequency cyclicity and regional depositional patterns of the Grayburg Formation, Guadalupe Mountains, New Mexico, *in* Meader-Roberts, S., Candelaria, M. P., and Moore, G. E., eds., Sequence Stratigraphy, Facies and Reservoir Geometries of the San Andres, Grayburg and Queen Formations, Guadalupe Mountains, New Mexico and Texas: Permian Basin Section SEPM Publication 91-32, p. 53-96.

Kerans, C., Nance, H. S., and Ye, M., 1992b, Recognition and Correlation of High-Frequency Cyclicity in Mixed Clastic-Carbonate Sequences: Reservoir Characterization Research

Laboratory-Characterization of Carbonate Ramp Reservoirs, Short Course October 11-14, 1992, Bureau of Economic Geology, The University of Texas at Austin, 54 p.

King, P. B., 1948, Geology of the southern Guadalupe Mountains: U.S. Geol. Survey Prof. Paper 215, 183 p.

Lucia, F. J., 1995, Rock-fabric/petrophysical classification of carbonate pore space for reservoir characterization: AAPG Bull., 79, p. 1275-1300.

Moran, W. R., 1954, Proposed type sections for the Queen and Grayburg Formations of Guadalupe age in the Guadalupe Mountains, Eddy County, New Mexico [abs.]: Geol. Soc. Amer. Bull., v. 65, p. 1288.

Naiman, E., 1982, Sedimentation and diagenesis of a shallow marine carbonate and siliciclastic shelf sequence: the Permian (Guadalupian) Grayburg Formation, southeastern New Mexico: unpublished M.A. thesis, The University of Texas, Austin, 197 p.

Nance, H. S., 1992, Facies architecture and internal geometry of a mixed siliciclastic-carbonate depositional sequence: Grayburg Formation, Stone Canyon, New Mexico, *in* Tyler, N., Barton, M. D., Bebout, D. G., Fisher, R. S., Grigsby, J. D., Guevara, E., Holtz, M., Kerans, C., Nance, H. S., and Levey, R. A., Characterization of Oil and Gas Reservoir Heterogeneity: Final Report, DOE Contract No. DE-FG22-89BC14403, p. 40-88.

Read, 1985, Carbonate platform facies models: AAPG Bulletin, v. 69, p. 1-21.

Ross, C. A., and Ross, J. R. P., 1987, Late Paleozoic sea levels and depositional sequences, *in* Ross, C. A., and Haman, D., eds., Timing and depositional history of eustatic sequences: constraints on seismic stratigraphy: Cushman Foundation for Foraminiferal Research, Special Publication 24, p. 137-149.

Ruppel, S. C., and Bebout, D. G., 1995, Effects of stratal architecture and diagenesis on reservoir development in the Grayburg Formation: South Cowden field, Ector County, Texas: Fossil Energy, DOE/BC/14895-10, Bartlesville Project Office, 80 p.

Sarg, J. F., and Lehmann, P. J., 1986, Lower-Middle Guadalupian facies and stratigraphy, San Andres-Grayburg Formations, Permian Basin, Guadalupe Mountains, New Mexico, *in*

Moore, G. E., and Wilde, G. L., eds., Lower and Middle Guadalupian Facies, Stratigraphy, and Reservoir Geometries, San Andres-Grayburg Formations, Guadalupe Mountains, New Mexico and Texas: Permian Basin Section, SEPM Publication 86-25, p. 1-36.

Senger, R. K., Lucia, F. J., Kerans, C., and Ferris, M. A., 1991, Dominant control on reservoir-flow behavior in carbonate reservoirs as determined from outcrop studies, *in* Linville, B., Burchfield, T. E., and Wesson, T. C., eds., *Reservoir Characterization III*: Tulsa, OK, Pennwell, p. 107-150.

Sonnenfeld, M. D., 1991, High-frequency cyclicity within shelf-margin and slope strata of the upper San Andres sequence, Last Chance Canyon, *in* Meader-Roberts, S., Candelaria, M. P., and Moore, G. E., eds., Sequence Stratigraphy, Facies and Reservoir Geometries of the San Andres, Grayburg, and Queen Formations, Guadalupe Mountains, New Mexico and Texas: Permian Basin Section, SEPM Publication 91-32, p. 11-51.

Sonnenfeld, M. D., 1993, Anatomy of offlap: Upper San Andres Formation (Permian, Guadalupian), Last Chance Canyon, Guadalupe Mountains, New Mexico: New Mexico Society Guidebook, 44th Field Conference, p. 195-203.

Walker, D. A., Golonka, J., Reid, A., and Reid, S., 1995, The effects of paleolatitude and paleogeography on Late Paleozoic carbonate sedimentation in West Texas; Part II: Permian: West Texas Geological Society Bulletin, v. 34, p. 5-14.

Wang, F. P., Lucia, F. J., and Kerans, C., 1994, Critical scales, upscaling and modeling of shallow-water carbonate reservoirs: Society of Petroleum Engineers, 1994 SPE Permian Basin Oil and Gas Recovery Conference, Midland, TX, March 16-18, p. 765-774.